UNIVERSITY OF OKLAHOMA

GRADUATE COLLEGE

PREDICTIVE TRACKING SIMULATION AND TECHNIQUES FOR ALL-DIGITAL RADAR

A THESIS

SUBMITTED TO THE GRADUATE FACULTY

in partial fulfillment of the requirements for the

Degree of

MASTER OF SCIENCE

By

SAVANNAH PATE

Norman, Oklahoma

2021

PREDICTIVE TRACKING SIMULATION AND TECHNIQUES FOR
ALL-DIGITAL RADAR

A THESIS APPROVED FOR THE
SCHOOL OF ELECTRICAL AND COMPUTER ENGINEERING

BY THE COMMITTEE CONSISTING OF

Dr. Nathan Goodman, Chair

Dr. Justin Metcalf

Dr. Jay McDaniel

Acknowledgments

I would like to take this opportunity to thank my advisor and chair, Dr. Nathan Goodman. I am so grateful for all his guidance and support through my undergraduate and graduate studies. I learned so much from this research opportunity and the advice he gave me along the way.

I would also like to thank the other members of my committee, Dr. Justin Metcalf and Dr. Jay McDaniel. Both of these professors are so passionate about radar engineering, and they have helped me find my passion in this field. I would like to thank Dr. Paul Moses for his mentorship during my undergraduate research experience. I have so many wonderful colleagues and mentors at the Advanced Radar Research Center (ARRC) at the University of Oklahoma. I am truly grateful to have the chance to work with so many determined and insightful people. In particular, Russell Kenney, Alex Pham, Jon Knowles, Yoon Kim, and Ellie Langley were wonderful friends who helped me with this thesis and other projects throughout my graduate studies.

Finally, I would like to thank my family for their overwhelming support throughout my life and especially during my time at the University of Oklahoma. No matter if I was hundreds of miles away or working at their kitchen table during the pandemic, they always encouraged me to keep researching and achieving my goals.

Table of Contents

List of Figures

List of Tables

Abstract

All-digital radar architectures allow radar systems to operate with more flexibility. Multiple Input, Multiple Output (MIMO) radars are especially effective at identifying multiple targets. Combined with statistical predictive tracking techniques, All-digital radars can allocate antenna resources during future coherent processing intervals to improve target signal-to-noise ratio (SNR) over time.

This thesis describes the relationships and models that characterize an all-digital phased array. The cognitive radar system simulated in this thesis is adaptively divided into several transmitting sub-arrays that are all independently capable of aiming at multiple targets within the radar's range. This thesis also discusses predictive tracking strategies that allow the radar controller to continuously track multiple targets within the radar's range. It discusses the process of dividing an array while still maintaining a SNR above the detection threshold. This thesis also examines the limits on how many targets the simulated all-digital array can track over many coherent processing intervals. In general, the all-digital array was able to track more targets compared to a phased array that forms a single transmit and receive beam each CPI.

Chapter 1

Introduction

The word RADAR is an acronym that stands for RAdio Detection And Ranging. At the most basic level, a radar antenna emits a radio signal that reflects off a target. The radar system then analyzes the properties of the reflected signal to learn about the target's position and movement. James Clerk Maxwell theorized that these radio signals behave similarly to visible light and were capable of reflection and refraction. In the 1880s, Heinrich Hertz experimentally proved these theories to be true. Radio and visible light waves are both examples of electromagnetic radiation; although radio waves have much longer wavelengths and lower frequencies than visible light, they share many of the same properties. Techniques using radio wave reflection to detect and locate targets were further studied during the 1930s. During World War II, the United States, the United Kingdom, Germany, Japan, and many other countries began the development of rudimentary radar detectors, with varying degrees of success [1].

Radar systems have existed for nearly a century. During this time, signal generators, detectors, Field Programmable Gate Array (FPGA) technologies, and computing have all improved immensely. Phased arrays are a specific type of antenna system that have existed since the 1950s and are now widely used in communica-

tions, remote sensing, and defense. Instead of having a single radiating element, an antenna array consists of several radiating elements with comparatively lower transmit power. This allows the phased array to transmit and receive signals in specific directions. [2]. Phased array operation will be discussed in further depth in Chapter 2.1

1.1 Motivation

Traditional radar systems have a single transmit-receive element that regulates radar behavior. Modern semiconductor technology for signal transmission, reception, and processing is sophisticated and relatively low-cost. It is now possible to utilize a transmit-receive element on each antenna in an array [3]. An all-digital array has a transmit-receive element on each antenna. Additionally, each array element is independently capable of waveform generation and digitization. The digitization of every antenna within an array allows for every element to act independently, allowing for flexible operation.

A phased array's radiation pattern is in a conic beam. Within the main lobe of the beam, the reflected radar signal has the strongest gain on Signal-to-Noise Ratio (SNR). The radar's ability to form beams digitally allows for it to control multiple beams simultaneously. Some all-digital radar systems are capable of transmitting several unique waveforms for each transmit beam and measuring many targets simultaneously [2] [4].

The goal of this study is to model an all-digital phased-array system capable of tracking many targets over hundreds of coherent processing intervals. Radar track-

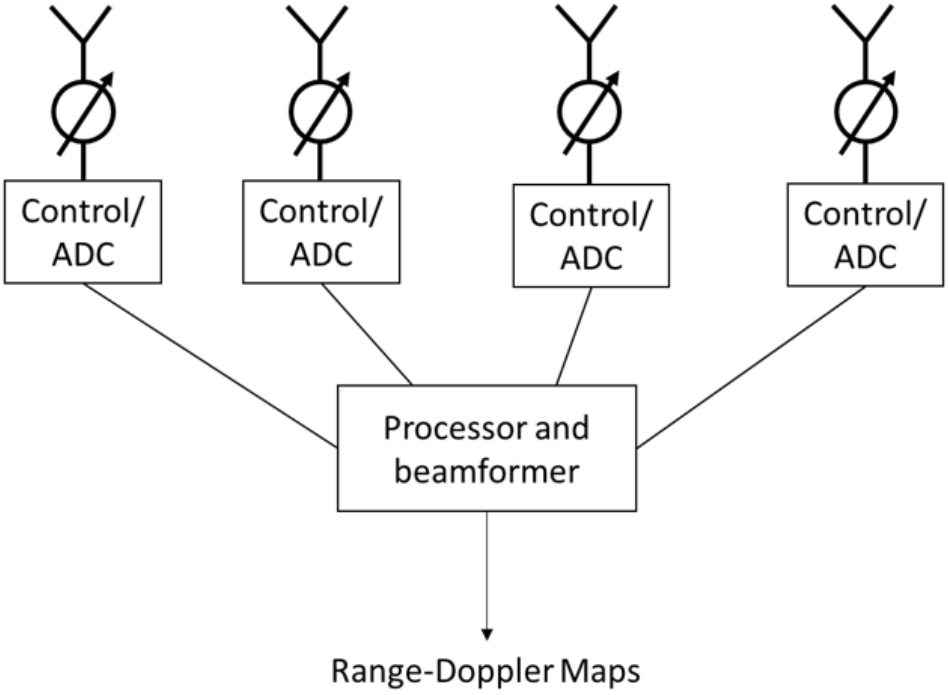

Figure 1.1: Architecture of a 1-D Phased Array

ing depends on the system's ability to make accurate measurements. For a reflected radar signal to have a strong enough SNR to be properly measured, the transmit and receive beams must be aimed at the target itself. Therefore, the radar must first have an estimate about a target's location, aim in the expected target direction, and update the target's location based on these measurements. For the purposes of this study, the radar is capable of dividing the entire phased array into sub-arrays. These sub-arrays form transmit and receive beams in the directions of specific targets. This simulation will test the limits of how many targets a divided phased array can track can be tracked by the system simultaneously compared to an array that only forms a single transmit and receive beam per coherent processing interval (CPI). The radar controller will have to decide how best to divide antenna resources and determine which targets have the strongest priority for measurement.

1.2 Thesis Outline

The remaining sections of this thesis are as follows. Chapter 2 reviews fundamental radar concepts. This chapter goes into detail about the mathematical models that govern all-digital phased arrays and describes Multiple-Input, Multiple-Output (MIMO) radar operation and waveform design. Chapter 3 overviews the main radar measurement simulation. The simulation models the transmission, reception, and processing of signals transmitted from a sub-divided digital array.

Chapter 4 overviews the predictive tracking process. This chapter details how the radar's controller makes an initial prediction and how future position and velocity predictions are affected by the radar's measurements. Chapter 5 describes the logic that governs the controller's decisions. The controller determines how to divide the array into different sub-arrays and determines the best aiming vectors for each transmit and receive beam.

Chapter 6 compares the performance of a divided MIMO array with that of an undivided array using the same tracking and metrics described in chapters 3 and 4. It also discusses the relationships between target signal-noise ratio, tracker confidence, and update frequencies. Chapter 7 shows the performance of the system as it tries to track an increasing number of targets with randomly generated paths. Chapter 8 concludes this thesis and summarizes the concepts that govern the simulation's operation.

Chapter 2

Background and Fundamentals

This chapter describes the mathematical relationships and models that characterize the behavior of a pulsed radar signal transmitted at a given target. The radar receiver will receive some modified version of the original pulse ($x(t)$). The pulse will be scaled, delayed, and phase-shifted according to target and environmental parameters. All of these effects can be described by well-known radar equations.

For a collocated radar system, where the receiver and transmitter are in the same location, the signal reflected off a target R_0 meters away reaches the receiver t_0 seconds later, where

$$t_0 = \frac{2R_0}{c}, \tag{2.1}$$

and c is the speed of light through free-space. It takes the radar signal R_0/c seconds to reach the target initially, and another R_0/c seconds for the reflected signal to reach the receiver. This study assumes that any target's movement during the time t_0 is negligible; this is often called the stop-and-hop assumption [5]. Measuring the time delay between signal transmission and reception allows the radar to determine the target's range (R_0).

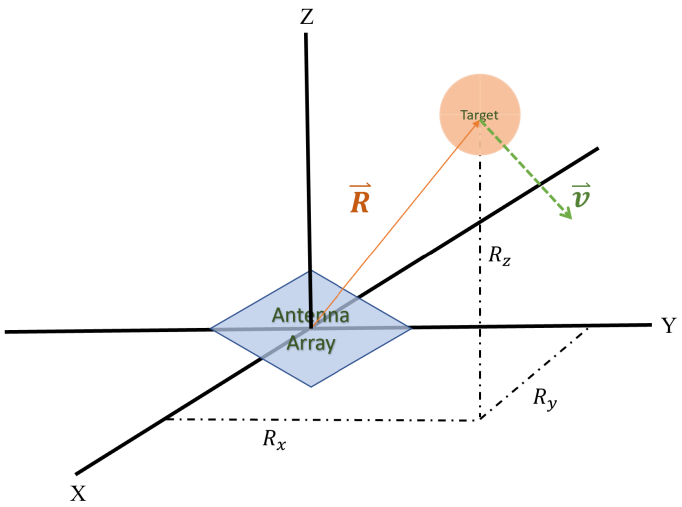

Figure 2.1: Basic Setup of a Collocated Radar Array

A target may be moving with some directional velocity $\hat{v}$. To measure this velocity, the radar emits multiple identical pulses and measures the target's velocity by analyzing the difference between each pulse's reflection. The delay between subsequent pulses is called the pulse repetition interval (PRI). The radar measures several pulses over a coherent processing interval (CPI).

A radar determines a target's speed by calculating the change in phase between subsequent pulses. For a target with a radial velocity of v relative to the radar system, the phase difference between each subsequent pulse, called the Doppler shift (F_d), is

$$F_d \approx \frac{2v}{\lambda}, \tag{2.2}$$

where λ is the wavelength of the pulse in meters. For a transmitted signal with a carrier frequency (F_c),

$$\lambda = c/F_c. \tag{2.3}$$

A physical S-band radar pulse is a real-valued analog signal modulated at some carrier frequency between 2-4 GHz. After the pulse's reception, it is downconverted to baseband. The carrier is removed so that the signal can be sampled at a rate corresponding to signal bandwidth (β).

For simulation purposes, it is often more useful to model the transmitted signal's complex envelope as

$$x(t) = a(t)\exp(j2\pi F_c t), \tag{2.4}$$

where $a(t)$ is an envelope function that will be explained further in section 2.2.

The received signal is a scaled, delayed version of $x(t)$. The mth received pulse can be modeled by

$$y(t,m) = \hat{a}(t-t_0)\exp[j2\pi F_c(t-t_0)]\exp[j2\pi m F_d] \tag{2.5}$$

where α is a scale factor. The reflected signal is weaker than the transmitted signal because of propagation loss and other factors described further in section 2.3.

2.1 Phased Array Considerations

Radar signals propagate through space as well as time; accounting for space propagation allows for the estimation of a wave's angle of arrival.

An all-digital phased array is comprised of multiple smaller antenna elements

with waveform generators. The waveform generators are able to delay the phase between adjacent elements, acting as a sort of phase shifter. While a single isotropic antenna radiates uniformly in all directions, an array of closely associated antennas can form a much narrower beam with a stronger gain in the center of the beam. The phase shifters on each antenna element allow the transmitter to steer the signal in the direction of a target, as explained below.

2.1.1 Spatial Propagation

The wavenumber (K) relates the number of wave cycles per distance traveled. A wave will travel 2π radians for each wavelength, but the wavelength depends on the signal's carrier frequency, leading to

$$K = \frac{2\pi}{\lambda} = \frac{2\pi F_c}{c}. \tag{2.6}$$

This expression means that as the wave moves through space, its phase will change by some amount related to the wavelength and the distance traveled. For the purposes of this study, we assume the waves are propagating in the three-dimensional Cartesian plane and free-space. We assume the array is in the $x - y$ plane at $z = 0$; the radar's broadside is in the positive z-direction. The wave vector $\bar{K}$ has a magnitude of K and is pointed in the direction of $\hat{r}$, the unit vector pointing from the array hardware to a target. Therefore, we have

$$\bar{K} = K\hat{r}, \tag{2.7}$$

where $\hat{r}$ is the unit vector pointing from the center of the antenna array to a target, and

$$\hat{r} = [r_x, r_y, r_z]. \tag{2.8}$$

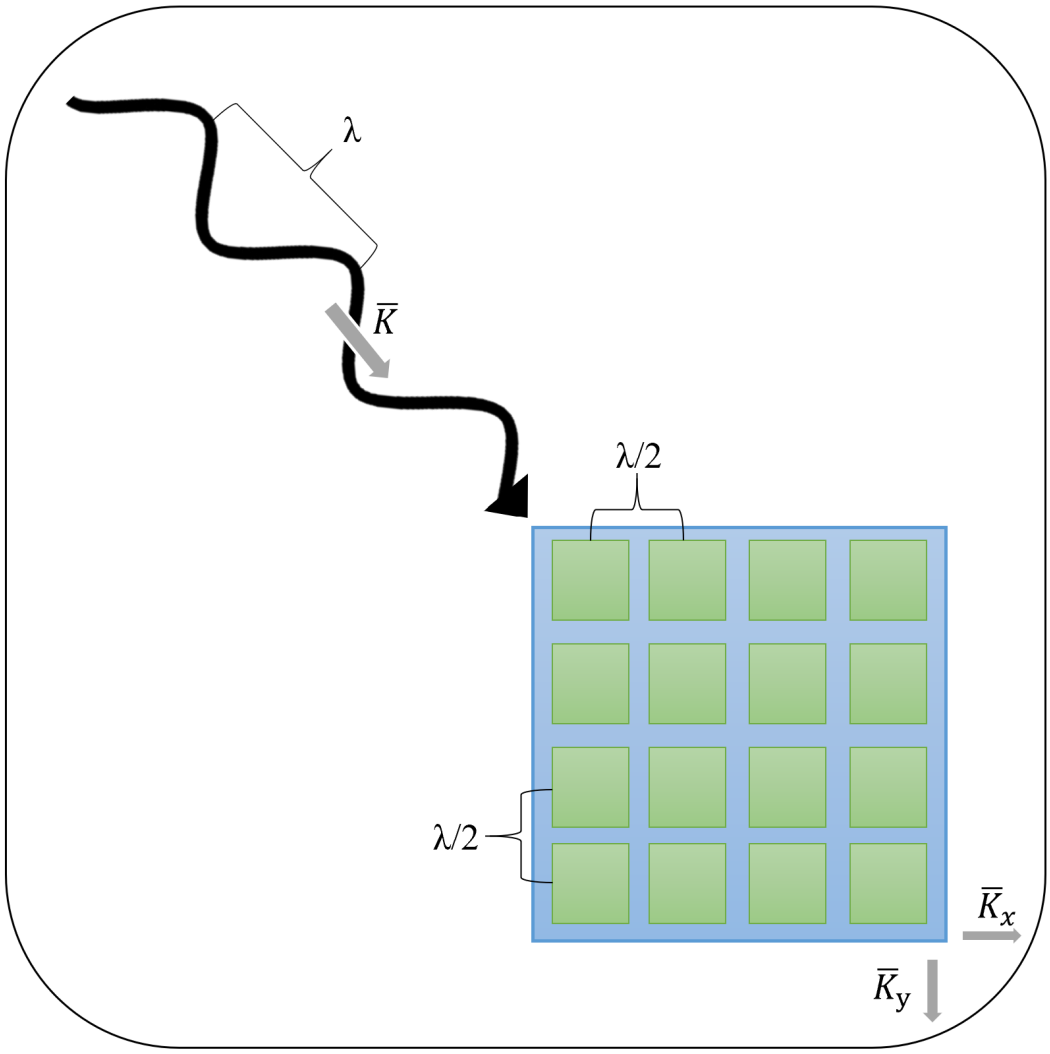

Figure 2.2: Spatial Sampling Visualization

The individual antennas are spaced $\lambda/2$ meters apart, as shown in Figure 2.2. Because the propagating wave must travel a different distance to each element, there

will be a phase shift between each element of the array. This phase shift is described by $\bar{K} \cdot \bar{r}$, where $\bar{r}$ is the unit vector pointing from the center of the antenna array to the antenna located at (x, y). Returning to (2.5), the mth pulse received by an antenna located at (x, y) will be modeled by

$$\tilde{y}(t, m, x, y) = \alpha x(t - t_0) \exp[j2\pi m F_d] \exp[j(\bar{K} \cdot \bar{r})]. \tag{2.9}$$

The radar will process the signal in (2.9) in order to determine a target's range, radial velocity, and spatial coordinates.

2.2 Pulse Structure

To determine the time delay between a pulse's transmission and reception, the received signal is passed through a matched filter [5]. The effectiveness of matched filtering is dependent on the pulse's auto-correlation. Ideally, the autocorrelation should be as low as possible at any delay other than zero seconds, where it should be maximized. Additionally, the peak in the autocorrelation should be narrow so that the matched filter has a fine range resolution. Finer resolution means that there is less ambiguity in the range measurement

The bandwidth of a simple square pulse with a duration of τ_p seconds is given by

$$\beta \approx 1/\tau_p. \tag{2.10}$$

The range resolution for a radar waveform with bandwidth β is given by

$$\Delta R = \frac{c}{2\beta} \approx \frac{\tau_p c}{2}, \tag{2.11}$$

which shows that shorter simple pulses have a finer range resolution. However, longer-duration pulses improve the received signal's energy and SNR. Using more complicated pulses, often called pulse compression waveforms, allows for finer range resolution without sacrificing pulse duration.

2.2.1 MIMO Radar

In order to exploit multiple antenna sub-arrays on transmit, an all-digital radar system must be able to transmit and receive several unique waveforms in close quarters. The radar waveforms should be highly auto-correlated but not strongly cross-correlated so that each matched filter can separate the signal from its corresponding transmit sub-array. [6]. Passing copies of the received signal through multiple filters is computationally complex, but it is important to identify from which sub-array the signal originated. For any phased array, the SNR is dependent on the number of antennas pointed at each target (this will be shown in (2.22)).

After each CPI, the radar tracker will update the predicted target locations and assign a certain number of antennas to point in that direction on the subsequent data collection.

MIMO radars have been extensively studied as an alternative to traditional phased arrays [7]. Generally, if a phased array is divided into sub-arrays, each sub-array can transmit a unique specific radar waveform. In a MIMO array, each radiating element is potentially capable of transmitting a unique radar pulse. Compared to traditional phased arrays, MIMO arrays can achieve narrower target resolutions and are more

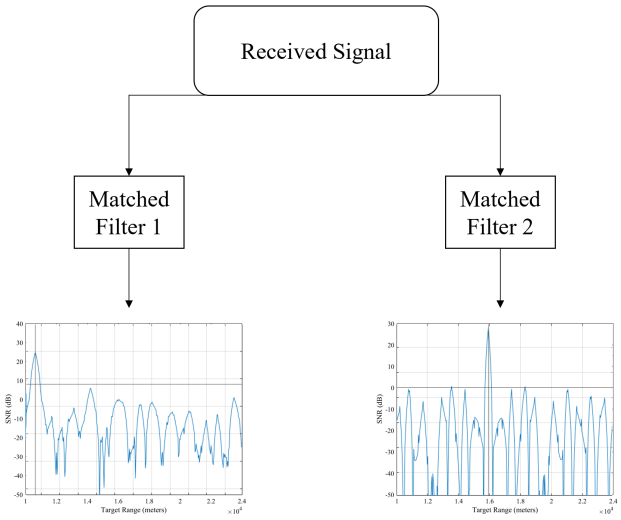

Figure 2.3: Results of multiple matched filters

sensitive to slow-moving targets [8]. Additionally, a MIMO radar transmitting M_t unique waveforms can detect up to M_t times as many targets as a traditional phased-array system. For the purposes of this study, MIMO radar is especially attractive. Element-level MIMO can be extremely computationally complex. The all-digital array simulation described in this thesis will reduce computational complexity by grouping the elements into transmitting sub-arrays [9] [10].

Waveform requirements for a MIMO radar are very flexible; the waveforms must be separable [8]. The ideal signals for a MIMO array are orthogonal to one another; each unique waveform should have no cross-correlation with other waveforms transmitted by the array. In practice, no set of waveforms is ideal for all ranges and Doppler shifts [11] [12]. Instead, determinations must be made concerning which waveforms have attractive properties for specific applications.

One method of waveform modulation for pulse compression is phase coding.

A phase-coded signal is separated into segments, or chips, of equal duration (τ_c) where

$$\tau_c = 1/\beta \tag{2.12}$$

for a signal with bandwidth β. The radio frequency of each chip is modulated by some discrete phase. Phase-coded signals are easy to generate and process. They tend to be strongly highly autocorrelated with a large main lobe peak to sidelobe ratio [13].

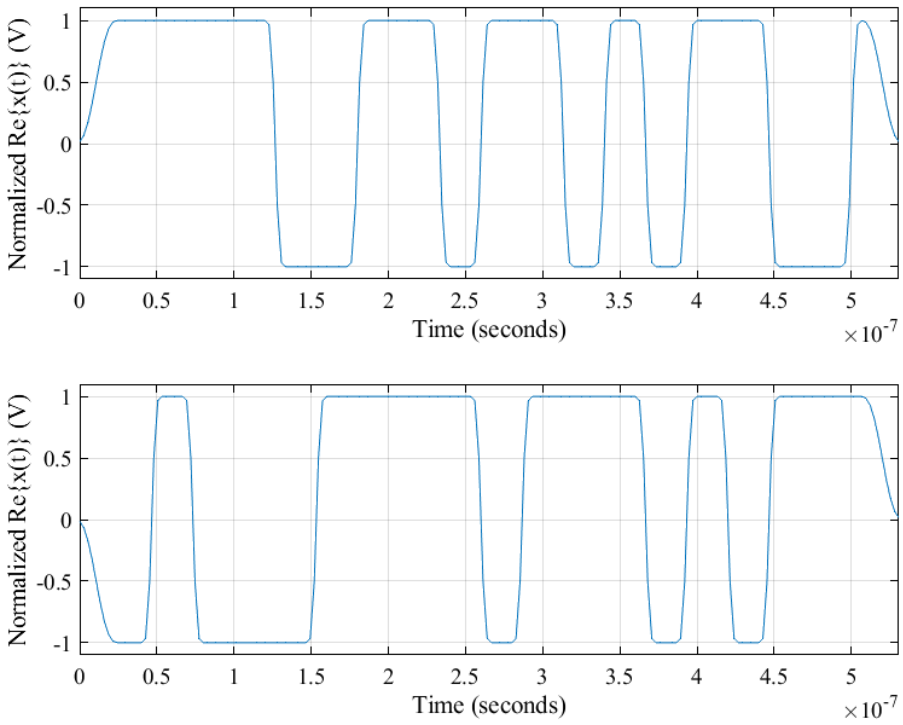

Figure 2.4: Two Binary Signals with $\tau_p\beta = 20$

Figure 2.4 shows the real parts of two different random biphase-coded waveforms, which have phase jumps between 0 and 180^o. The maximum number of unique codes that can be generated by this method is $2^{\tau_p\beta}$. As the number of unique

signals transmitted by an array approaches $2^{\tau_p\beta}$, the cross-correlation of the signals will increase because the individual codes will have more elements in common. This is not necessarily a concern as $2^{\tau_p\beta}$ will generally be much larger than the number of unique waveforms transmitted by a MIMO array.

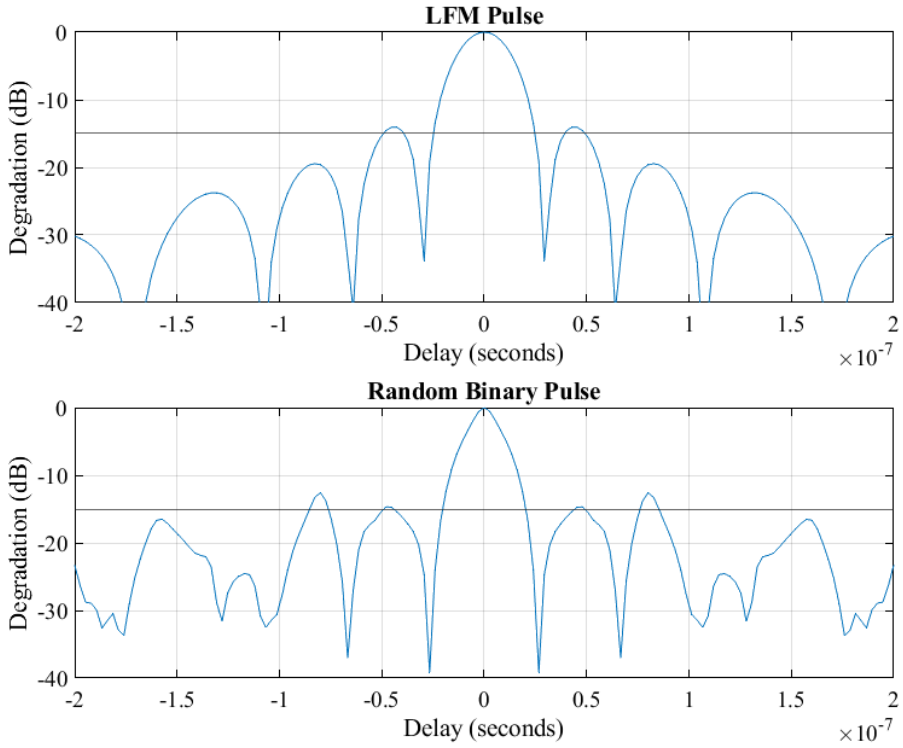

Figure 2.5: Auto-correlation of Radar Pulses with $\tau_p\beta = 20$

As Figure 2.5 shows, a pulsed signal's maximum autocorrelation occurs at a delay of $\tau = 0$. For the purposes of matched filtering, this means that the received signal will have a strong peak at a delay corresponding to $2R_0/c$. Outside of that peak, the signal power will be suppressed. When the autocorrelation has strong peaks at delays other than $\tau = 0$, signals outside of the expected matched filter return may not be suppressed, causing false alarms or detections at inaccurate target

ranges. These peaks are known as sidelobes.

Binary phase-coded signals are not the most efficient pulse-compression waveforms in terms of peak sidelobe level or power efficiency. Linear frequency modulated, or LFM, signals are widely used in radar and communication because they tend to have weak sidelobes. Figure 2.5 shows the autocorrelation of an LFM and a biphase-coded signal with the same time-bandwidth product. The biphase coded signal has stronger sidelobes.

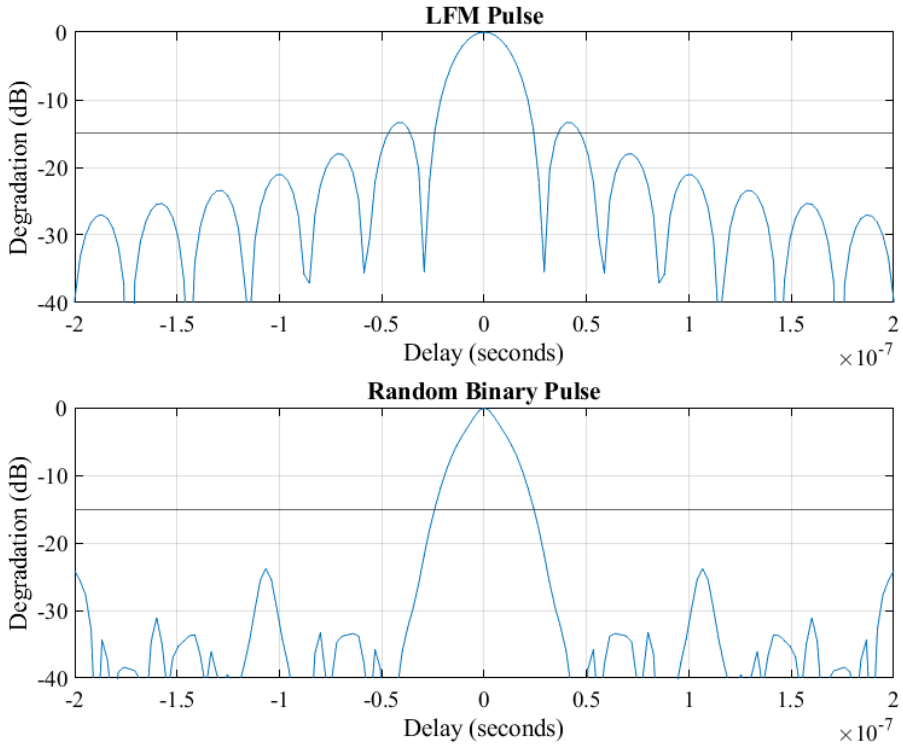

Figure 2.6: Autocorrelation of Radar Pulses with $\tau_p\beta = 750$

The poor performance of the 20-chip pseudorandom binary sequence (PRBS) pulse can be improved by increasing the number of chips, or the time-bandwidth

product. Figure 2.6 shows the autocorrelation of an LFM with $\tau_p\beta = 750$ and a random binary pulse with 750 chips. The signals in figure 2.6 have the same bandwidth and therefore the same resolution as the signals in 2.5; the pulse duration increased in 2.6. The difference in performance between the random binary signal and the LFM signal is less noticeable; both signals have fine resolutions and their sidelobes are generally at least 15dB below the maximum. The random binary signal has a better peak sidelobe level than the LFM signal, meaning that it would perform better in the matched filter. Therefore, PRBS signals with a large time-bandwidth product are suitable for this study.

As Figure 2.7 shows, the more chips a binary pulse has, the lower its cross-correlation with other signals. Lower cross-correlations mean that each matched filter should separate results based on the corresponding transmitted signal; the matched filter should suppress results from the other waveforms.

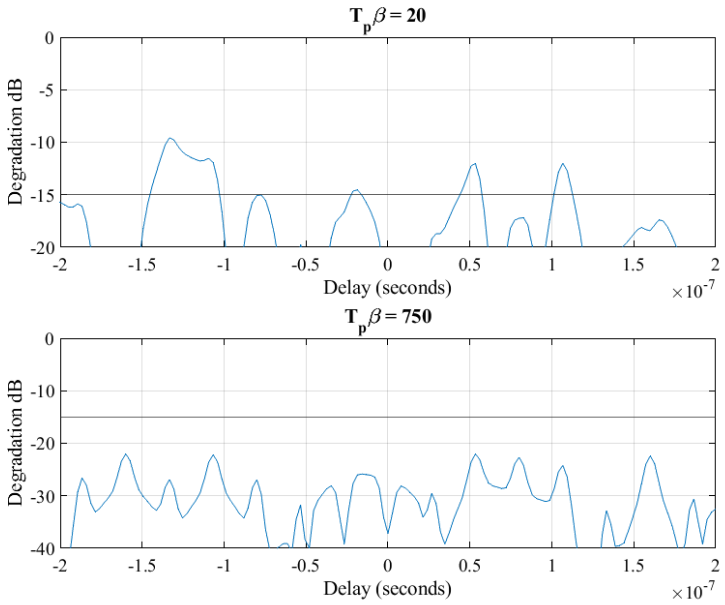

Figure 2.7: Example of the Cross-Correlation between PRBS

As $\tau_p\beta$ increases, PRBS waveforms' sidelobe levels and cross-correlation decrease. However, increasing bandwidth is not always possible. Increases a radar signal's pulse durations can limit its pulse repetition frequency. Since the maximum radial velocity that can be measured by a radar (v_{ua}) with a pulse repetition frequency of f_{PRF} is given by

$$v_{ua} = \frac{\lambda f_{PRF}}{4}, \tag{2.13}$$

increasing τ_p may interfere with a radar's ability to measure fast-moving targets velocities [5]. Furthermore, in a simulated radar, increasing τ_p or β increases the computational complexity of modeling signal transmission, reception, and processing.

2.3 Thermal Noise and Signal-to-Noise Ratio

Additive thermal noise is a major issue with the accuracy of radar measurements. Because noise lacks a clear pattern, it is very difficult to remove it completely. The average noise power (P_n) of a radar signal is

$$P_n = k_b T F_s F_{sys}, \tag{2.14}$$

where k_b is Boltzmann's constant, T is the system temperature (assumed to be 290K at room temperature), F_s is the analog-to-digital converter's (ADC's) sampling frequency, and F_{sys} is the system's noise figure.

For the radar to be able to detect a target, its post-processed signal power must be stronger than the noise floor. Each antenna in this phased array simulation has a

low transmit power. Pulse compression, Doppler processing, and digital beamforming increase the post-processing signal power so that the radar system can detect many targets. The SNR also helps establish the interval of confidence in the target parameter measurement discussed in Section 4.1.

2.3.1 Signal Power Fundamentals

The received signal power (P_r) reflected off a target and received by the radar receiver is modeled by

$$P_r = \frac{N_t P_t G_t G_r \lambda^2 \sigma}{(4\pi)^3 R^4}, \tag{2.15}$$

where σ is the target's radar cross-section. P_t is the signal power, in watts, transmitted from each individual antenna, N_t is the number of transmitting antennas, and G_t and G_r are the antenna gains on transmit and receive, respectively. (2.15) is the standard radar range equation [5]; the overall transmitting power is the transmitting power of a single antenna multiplied by the total number of transmitting elements.

For the purposes of this project, small groups of antennas may transmit unique pulses, but the reflected pulses will be received by the entire array.

2.3.2 Transmit Beam Steering

Beam steering increases the gain on the received voltage by the array factor F, which is dependent both on the number of array elements and the accuracy of the aiming vector. $\bar{r}$ is the unit vector pointing from the center of the antenna array to

the antenna located at (x, y). For a transmitting antenna array with N elements,

$$F(\bar{K}_{aim}) = \sum_{i}^{N_t} \exp\left[j(\bar{K} - \bar{K}_{aim}) \cdot \bar{r}_i\right] = k_t N_t. \tag{2.16}$$

When $\bar{K}_{aim} = \bar{K}$,

$$F(\bar{K}_{aim} = \bar{K}) = \sum_{i}^{N_t} \exp\left[j(0) \cdot \bar{r}_i\right] = N_t. \tag{2.17}$$

In this case, F is equal to the number of transmitting antenna elements, N_t. Thus, the array factor increases with the number of transmitting antennas and the accuracy of the aiming vector [14].

The array factor scales the signal's voltage, so the received signal's power is related to k_t^2. Specifically in (2.15),

$$G_t = G_a k_t^2 N_T. \tag{2.18}$$

Assume each individual antenna in the array has a gain of G_a on both transmit and receive. Therefore,

$$P_r = k_t^2 G_a N_t^2 \frac{P_t G_r \lambda^2 \sigma}{(4\pi)^3 R_0^4}. \tag{2.19}$$

2.3.3 Reception Beamforming

When a radar switches from transmitting mode to receiving mode, it stops emitting waves and instead detects reflected signals. A phased array forms narrow receiver beams focused in a single direction. Figure 2.8 shows the antenna pattern of a linear phased array where the antennas are at a distance of $\lambda/2$ apart from one

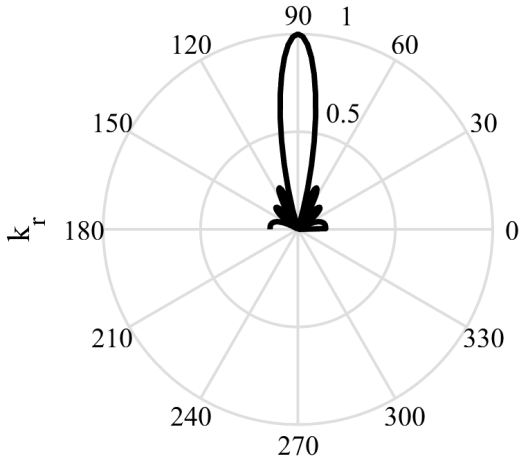

Figure 2.8: Beam Pattern of a 1-D phased array aimed at 90^o

another. The front lobe of the beam is pointed at 90^0. If a target was at exactly 90^o, that target would have an additional gain equal to N_r.

If the target was slightly misaligned with the beam peak, it would have a gain of $k_r N_r$. Arrays have small sidelobes as well, such as the ones at 180^o and around 70^o. These sidelobes mean that targets not exactly in the main beam can have a small gain, but all of these sidelobes have a $k_r < 0.1$

Much like with transmitted signals, the phased array can apply some phase shift to these receiver beams to point them in a specific direction. Figure 2.9 shows the array described above but aimed at an angle of 120^o rather than broadside.

Antenna arrays are capable of forming multiple beams simultaneously. This can be done by Fast-Fourier-Transform (FFT) processing; performing an FFT across the received signal is the same as forming all possible beams in an antenna array.

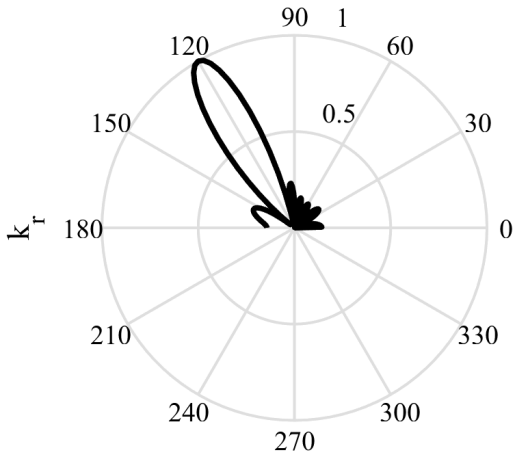

Figure 2.9: Beam Pattern of a 1-D phased array aimed at 120^o

Theoretically, the radar can form as many beams as there are antennas in the array. This would be a considerable amount for a physical radar to handle. Instead, it is more effective to form a set of beams in a few specified directions. Figure 2.10 shows the pattern of an array forming beams at 90^o, 130^o, and 70^o. The gain on the 90^o and 130^o beams do not have a maximum k_r of 1, but they are very close.

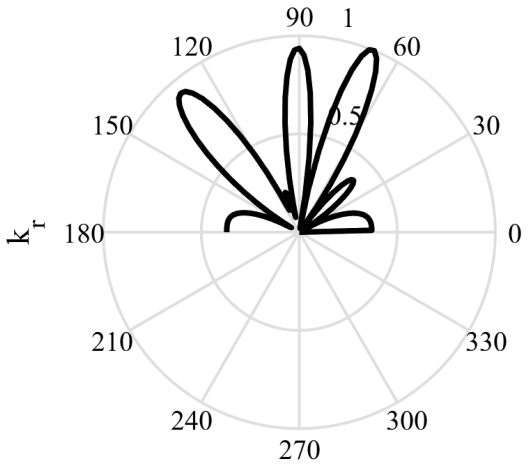

Figure 2.10: Array Pattern and Response to Multiple incoming Signals

Forming a receiver beam in direction $\hat{r}$ is described by

$$\tilde{y}(t, m, \hat{r}_x, \hat{r}_y) = \sum_{i=1}^{N_x} \sum_{l=1}^{N_y} y(t, m, r_{yl}, r_{xi}) \exp\Big[-j\pi(i-1)\hat{r}_x\Big] \exp\Big[-j\pi(l-1)\hat{r}_y\Big]. \tag{2.20}$$

If a receiver beam is not formed exactly in the direction of the target, k_r decreases. Assuming that the steering vector is fairly accurate, the receiver beam should have a $k_r \approx 1$.

After signal reception, phased array signal processing improves the signal power by a factor of $\tau_p \beta M$; the overall radar gain on receive is

$$G_r = \tau_p \beta M N_r G_a. \tag{2.21}$$

Replacing G_r with (2.21), each received target should have a measured SNR value described by equation

$$SNR = N_t^2 k_t^2 N_r \tau_p \beta M \frac{P_t G_a^2 \lambda^2 \sigma}{(4\pi)^3 R_0^4 P_n}. \tag{2.22}$$

Chapter 3

All-Digital Phased Array Radar Simulation

This chapter gives a detailed description of the MATLAB simulation that was developed to model the behavior of an adaptive all-digital MIMO array system. The radar array consists of several rectangular (or L-shaped, as discussed in Section 5.2) sub-arrays. Every antenna possesses its transmit-receive element and is capable of producing a unique waveform. Antenna elements grouped in the same sub-array transmit the same waveform. Each sub-array transmits a different random-binary pulsed signal at a common carrier frequency, pulse duration, and bandwidth. Additionally, each transmitting sub-array can have a unique aiming vector if necessary.

3.1 Overview

Although each target will reflect a portion of each transmitted waveform, k_t and k_r will severely degrade if a beam is not pointed at a target [8]. This should limit some interference due to having multiple targets in a constrained volume.

Each target in this simulation has a randomly generated original position and velocity and has a small random acceleration with a predetermined variance, as well as a randomly determined radar cross-section (RCS). The target paths are generated

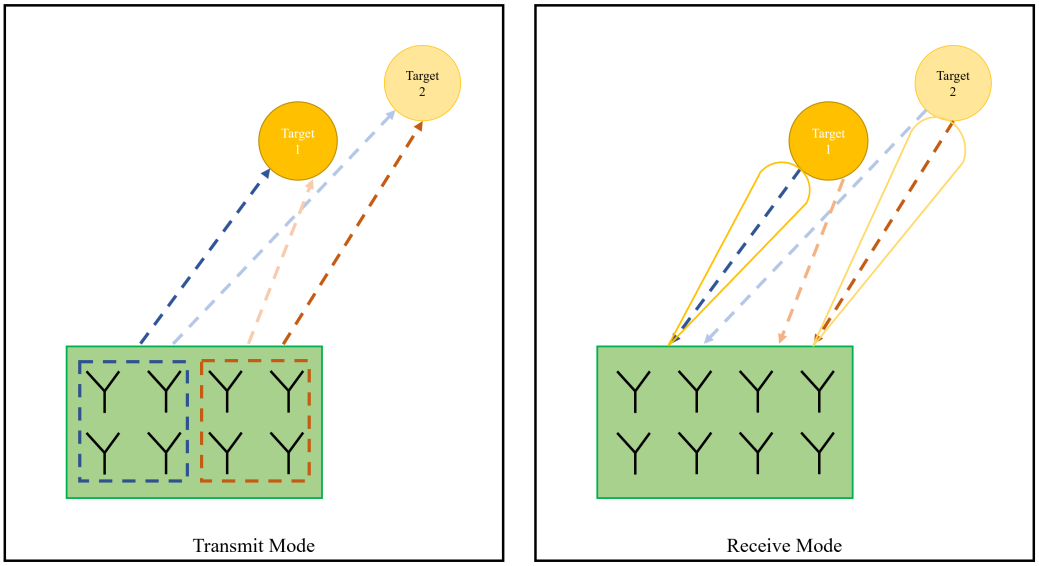

Figure 3.1: Transmitted MIMO Signal Reflections

such that each target remains within a distance that is well within the unambiguous range that can be measured by the radar. Additionally, each target travels with a velocity that can be unambiguously measured by the system. The radar scheduler determines reconfigurable transmitting sub-arrays as will be described in Section 5.1. The antenna array in this simulation is a square array of 32 x 32 antennas. The antenna spacing is $\lambda/2$ in both dimensions.

The received signal is modeled as the sum of all the scaled and delayed signals reflected off each target. The signals are also multiplied by a phasor to simulate Doppler shift and the number of wavelengths traveled between the array and each target, as described in the previous chapter. There is also Gaussian random noise with a strength determined by the system's noise figure. A copy of each transmitted waveform is saved for matched filter processing.

The received signal is first Doppler processed using an FFT. Then, the receiver

digitally forms 16 beams around each aiming vector according to (2.20). Copies of the beamformed signal are passed through each matched filter [7]. The resultant signals are 4-dimensional with a dimension corresponding to range, radial velocity, and spatial frequencies in x and y. Some "slices" containing a target are shown in Figures 3.2 and 3.3. The simulation searches for peaks in the post-processed SNR map to determine target parameters.

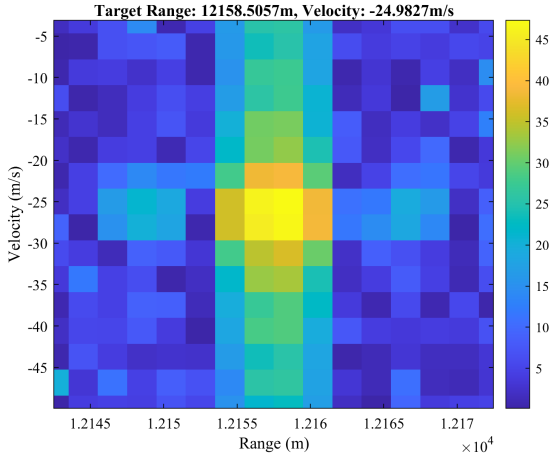

Figure 3.2: Post-Processing Range-Velocity Map

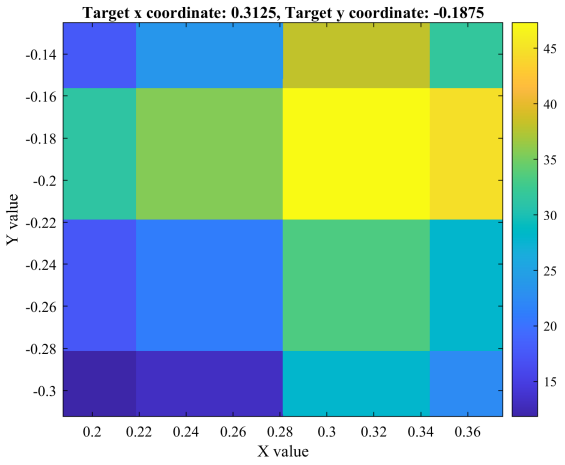

Figure 3.3: Post-Processing X-Y Map

3.2 Interpolation

Figure 3.3 shows an array slice that contains the 16 slightly offset beams formed around the aiming vector. Because at least one beam has an SNR of at least 15dB, there is likely a target within one of them. However, further processing must be done to determine accurate target parameters. Each beam has a width of $2/32 = 0.0625$. Because the brightest cells are in the column corresponding to $r_y = -0.1875$, there is a good chance that a target is in that direction. However, there are two bright adjacent cells in the r_x direction. The target could theoretically be in either of those beams and is likely between them.

Consider Figure 3.4. If the receiver forms beams centered at 70^o and 90^o because of hardware limitations, a target at 80^o would have at least 10^o error on its measurement because the receiver searches for the strongest beam return and there is no beam pointed at 80^o. The radar measurement can only be as accurate is as its resolution. At long ranges, a small unit vector difference can cause a fairly large difference in Cartesian position.

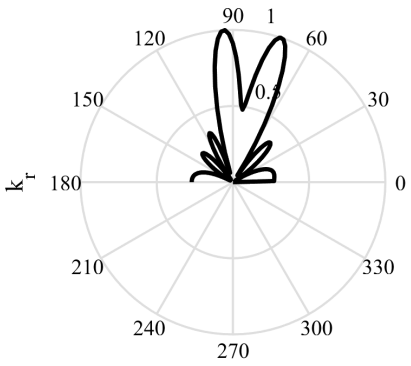

Figure 3.4: Array Response with two adjacent receiver beams

To combat this, interpolation was performed on the range-Doppler-angle map as shown in Figures 3.5 and 3.6. Figure 3.5 is an interpolated version of Figure 3.2 and Figure 3.6 is an interpolated version of Figure 3.3. In this example, r_y is still -0.1875, but r_x actually has a value of 0.32031.

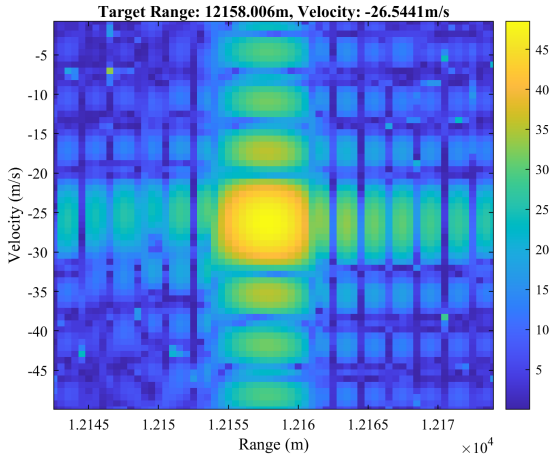

Figure 3.5: Interpolated Range-Velocity Map

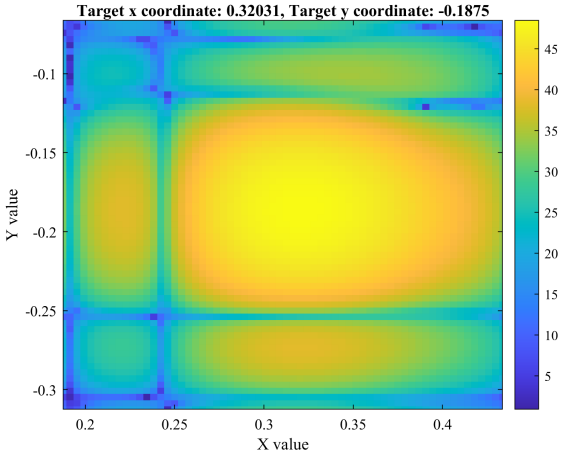

Figure 3.6: Interpolated X-Y Map

The peak value in the 4-D interpolated Range-Velocity-Angle map corresponds to the target's location and radial velocity. The maximum value in the map is related to the target's SNR. The target's range, velocity, and x and y unit vectors are recorded along with $SNR_1 = SNR/N_t^2$. A target's SNR depends on the number of transmitting antennas, as described in Section 2.3. This simulation uses the peak value in the post-processed received signal to estimate SNR_1, the theoretical SNR of the target if a single transmitting antenna is aimed at it. The MIMO array's controller will adjust the number of transmitting elements focused on a target such that $SNR_1 N_T^2$ is high enough to reach the detection threshold

In Section 2.2.1, the random biphase-coded random pulses had a peak sidelobe level at least 15dB lower than the mainlobe when $T_p\beta = 750$. This means that post-processing array cells with a value less than 15dB above the noise floor are likely sidelobes or noise. Furthermore, Figure 3.7 shows a strong matched filter output from a target around 18Km away from the radar. The signal power around the target's actual range is above the noise floor. Sidelobe power increases as signal power increases. To avoid sidelobe detections, the signal processor ignores peaks that are less than 15dB below the maximum signal power.

If a cell in Figures 3.2 and 3.3 lies above the threshold, that cell is considered a detection.

In a real radar system, the true range, velocity, and unit vector of the target are not known. The radar would have to determine which detection is most likely to correspond to the target's parameters. Because this is a simulation, the true target parameters are known. Rather than performing the difficult task of target associa-

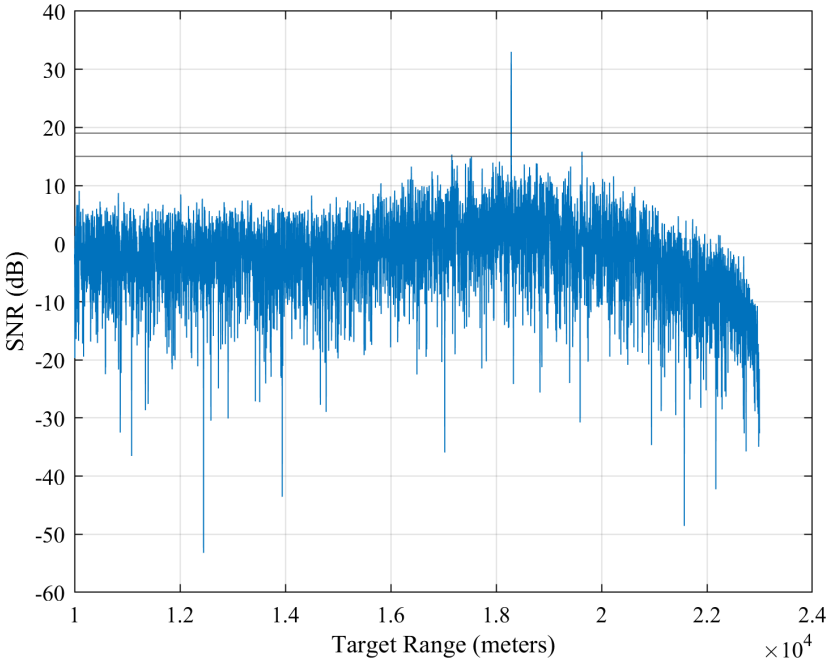

Figure 3.7: Matched filter with noticeable sidelobes

tion, the radar saves the detections that are closest to the targets' actual locations and radial velocities.

Figure 3.8 shows a range slice of a single beam in the post-processed signal. Two targets lie in this beam; they are at the same azimuth and elevation but different ranges. The nearer and weaker target lies outside the sidelobes of the stronger and farther target. In this example, the radar would have detected the farther target first. Because that target has a normalized SNR of approximately 35dB, the simulation would then look for any targets stronger than 20dB above the noise floor. The simulation ignores any peaks within 2 resolutions ($c/2\beta$) of previous detections. The smaller SNR spike is stronger than 20dB above the noise floor, so the simulation examines it to determine another target's parameters.

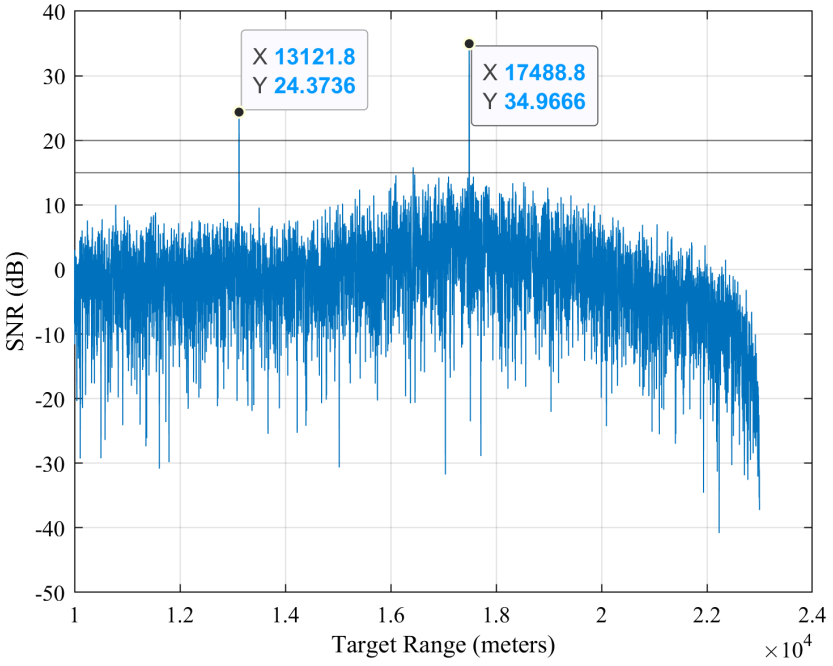

Figure 3.8: Matched Filter with multiple targets

Although the strongest cell in the array should correspond to the target at which the transmitting sub-array was aimed, some of the transmitted signal could be reflected off other targets. If a transmitting sub-array has a lot of antennas, SNR may be very strong even if k_t is small. Ideally, $k_t \approx 1$. If $k_t = 0.6$, $k_t^2 = 0.36$, which is a 5dB drop compared to $k_t = k_t^2 = 1$. The radar records any target detection, whether or not a sub-array was intentionally aimed at that target. The radar system's processor and controller will use the measured values to refine the aiming vector for subsequent CPIs. This prediction process is described in more detail in the next chapter.

Chapter 4

Predictive Tracking

Traditional radars consist of some form of antenna emitting a pre-determined signal and listening back for that signal's echo; repeating this process to gather target information. In this context, the collection of information is performed in a rigid, pre-defined manner.

Advances in computing allowed radar controllers to mimic the cognitive process; a capability widely sought by engineers since the 1930s. Machine learning depends on a machine's observations and the degree of confidence in these observations to make decisions about what to do next. The idea of cognitive radar is especially promising; all-digital radars have many dynamic parameters that can be managed by a radar's controller. For example, the controller could determine how to divide a radar system's power and/or antenna resources to ideally track many targets [15, 16].

Cognitive, or fully adaptive radar systems utilize feedback loops like that pictured in Figure 4.1. The radar optimizer and processor examine measurement data to make decisions about if and how to change the radar's operating parameters. In this thesis, the main operating parameter controlled by the radar system is the

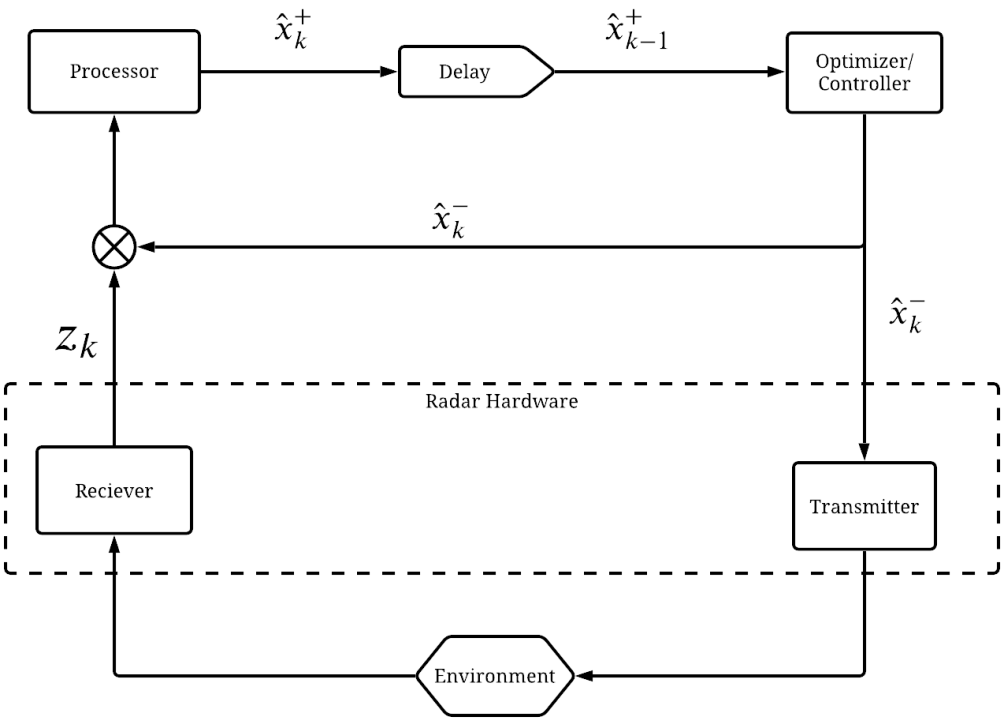

Figure 4.1: Sample Architecture of a Cognitive Radar

number of antenna elements allocated to each target. A typical array may have thousands of antenna elements that can be controlled. This chapter describes the processes by which a radar controller may decide how to divide its limited antenna resources to maintain as many target tracks as possible.

4.1 Kalman Filtering

Because the array factor depends on the accuracy of the steering vector, it is important for the radar system to accurately predict the target's direction. One method of predicting target motion is Kalman filtering. A Kalman filter generates a least-squares estimate of a dynamic system's state as it changes over time. The filter compares the confidence in its initial estimate with the confidence in a measured

value. The Kalman filter then uses these confidence measurements to update the state's posterior estimate. A Kalman filter operates under the assumption that the dynamic system is linear and has additive Gaussian noise. [17]

Let $\mathbf{x}_k$ be a state vector at iteration k of the Kalman filtering algorithm. For the purposes of the target tracking algorithm in this thesis, $\mathbf{x}_k$ is a column vector containing a target's position and velocity data, where

$$\mathbf{x} = \begin{bmatrix} x & y & z & V_x & V_y & V_z \end{bmatrix}^T. \tag{4.1}$$

The Kalman filter assumes

$$\mathbf{x}_k = \mathbf{F}\mathbf{x}_{k-1} + \mathbf{w}_k \tag{4.2}$$

where

$$\mathbf{F} = \begin{bmatrix} 1 & 0 & 0 & dt & 0 & 0 \\ 0 & 1 & 0 & 0 & dt & 0 \\ 0 & 0 & 1 & 0 & 0 & dt \\ 0 & 0 & 0 & 1 & 0 & 0 \\ 0 & 0 & 0 & 0 & 1 & 0 \\ 0 & 0 & 0 & 0 & 0 & 1 \end{bmatrix} \tag{4.3}$$

is the state transition matrix for a target moving with constant velocity, dt is the interval between consecutive measurements, and $\mathbf{w}_k$ is additive Gaussian noise. Although the F matrix assumes that the velocity is constant, there is actually a small acceleration with a Gaussian random variance of σ_a^2. This acceleration represents

the dynamic nature of the system and is injected via the process noise vector $\mathbf{w}_k$ [18–20]. $\mathbf{w}_k$ has a covariance matrix of $\mathbf{Q}$, where

$$\mathbf{Q} = \begin{bmatrix} 0 & 0 & 0 & 0 & 0 & 0 \\ 0 & 0 & 0 & 0 & 0 & 0 \\ 0 & 0 & 0 & 0 & 0 & 0 \\ 0 & 0 & 0 & \sigma_a^2 dt^2 & 0 & 0 \\ 0 & 0 & 0 & 0 & \sigma_a^2 dt^2 & 0 \\ 0 & 0 & 0 & 0 & 0 & \sigma_a^2 dt^2 \end{bmatrix} \tag{4.4}$$

.

The Kalman filter provides a least-squares estimate of the state vector $\mathbf{x}$. Before each CPI, the radar system predicts a target's position and velocity using

$$\hat{\mathbf{x}}_k^- = F\hat{\mathbf{x}}_{k-1}^+. \tag{4.5}$$

After a measurement is made, the filter uses the measurement vector $\mathbf{z}$, where

$$\mathbf{z} = \begin{bmatrix} r_x & r_y & R & V_r & V_x & V_y & V_z \end{bmatrix}^T \tag{4.6}$$

to update the estimated position and velocity based on the confidence in the initial prediction ($\hat{\mathbf{P}}$) and the confidence in the measurement ($\mathbf{R}$), according to the Kalman filter equations. The a priori estimate of $\mathbf{P}$ is determined by the posterior estimate of $\mathbf{P}$ from the previous CPI and the plant noise ($\mathbf{Q}$), according to

$$\hat{\mathbf{P}}_k^- = \mathbf{F}\hat{\mathbf{P}}_{k-1}^+\mathbf{F}^T + \mathbf{Q}. \tag{4.7}$$

The hat operator indicates predicted values; the superscripts of + and - indicate posterior and a priori predictions respectively. $\hat{\mathbf{P}}$ is the error covariance of $\hat{\mathbf{x}}$; smaller values of $\hat{\mathbf{P}}$ suggest that $\hat{\mathbf{x}}$ is a more accurate prediction.

The Kalman gain ($\mathbf{K}$) compares the confidence in the priori state estimate to the confidence in a measurement and is defined by

$$\mathbf{K} = \frac{\hat{\mathbf{P}}_k^- \mathbf{H}^T}{\mathbf{H}\hat{\mathbf{P}}_k^- \mathbf{H}^T + \mathbf{R}} \tag{4.8}$$

where $\mathbf{H}$ is a linear transform matrix based on $h(\mathbf{x})$, the relationship between the state and measurement vectors. The next section will describe $\mathbf{H}$ and $h(\mathbf{x})$ in more detail.

The Kalman gain is used to estimate each measurement's accuracy and to update the posterior state vector estimate according to

$$\hat{\mathbf{x}}_k^+ = \hat{\mathbf{x}}_k^- + \mathbf{K}(\mathbf{z}_k - h(\hat{\mathbf{x}}_k^-)). \tag{4.9}$$

As $\mathbf{K}$ increases, the posterior state estimate approaches $h^{-1}(\mathbf{z}_k)$. The state estimate error covariance is adjusted to reflect the posterior state estimate according to

$$\hat{\mathbf{P}}_k^+ = (\mathbf{I} - \mathbf{K}\mathbf{H})\hat{\mathbf{P}}_k^-. \tag{4.10}$$

As $\mathbf{K}$ increases, $\hat{\mathbf{P}}_k^+$ decreases, indicating that the Kalman filter is very confident in the posterior state estimate $\hat{\mathbf{x}}_k^+$ [17].

4.1.1 Nonlinear Measurement Updates

The radar modeled in this thesis does not measure the state $\mathbf{x}$ directly. Instead, it measures the x and y components of the unit vector (r_x and r_y) pointing from receiver to the target, the range to the target, R, and the scalar target speed relative to the receiver, $V_r = \hat{r} \cdot \bar{v}$.

Each component of the unit vector $\hat{r}$ can be found unambiguously. r_x and r_y are directly measured by the radar. r_z is determined by

$$\sqrt{r_x^2 + r_y^2 + r_z^2} = 1$$

$$r_z = \pm\sqrt{1 - (r_x^2 + r_y^2)} \tag{4.11}$$

The positive z direction is defined as straight in front of the array; $\hat{r}_z$ must be positive as the radar cannot measure targets behind it.

Although $\hat{r}$ and V_r are known, it is impossible to find the inverse of the dot product of two vectors; however, the actual velocity vector cannot be directly determined. The individual components of $\bar{V}$ can be indirectly estimated by $V_x = \hat{V}_x + \Delta v$, $V_y = \hat{V}_y + \Delta v$, $V_z = \hat{V}_z + \Delta v$. Δv is determined by

$$\hat{V}_r = \frac{\hat{x}\hat{V}_x + \hat{y}\hat{V}_y + \hat{z}\hat{V}_z}{\sqrt{\hat{x}^2 + \hat{y}^2 + \hat{z}^2}}$$

$$V_r = \hat{r}_x V_x + \hat{r}_x V_y + \hat{r}_z V_z$$

$$= \hat{r}_x(\hat{V}_x + \Delta v) + \hat{r}_y(\hat{V}_y + \Delta v) + \hat{r}_z(\dot{\hat{V}}_z + \Delta v)$$

$$= \hat{r}_x\hat{V}_x + \hat{r}_x\Delta v + \hat{r}_y\hat{V}_y + \hat{r}_y\Delta v + \hat{r}_z\hat{V}_z + \hat{r}_z\Delta v$$

$$V_r = \hat{V}_r + \Delta v(\hat{r}_x + \hat{r}_y + \hat{r}_z)$$

$$\Delta v = \frac{V_r - \hat{V}_r}{\hat{r}_x + \hat{r}_y + \hat{r}_z} \tag{4.12}$$

.

The Kalman filter assumes that the measurement vector is some linear transform $h(\mathbf{x})$ of the current state vector plus some Gaussian measurement noise $\mathbf{v}$,

$$\mathbf{z}_k = h(\mathbf{x}_k) + \mathbf{v}_k \tag{4.13}$$

In this case, however, $h(\mathbf{x})$ is not linear and does not hold with Kalman filtering assumptions. Instead,

$$h(\mathbf{x}) = \begin{bmatrix} \dfrac{x}{\sqrt{x^2+y^2+z^2}} \\ \dfrac{y}{\sqrt{x^2+y^2+z^2}} \\ \sqrt{x^2+y^2+z^2} \\ \dfrac{xV_x + yV_y + zV_z}{\sqrt{x^2+y^2+z^2}} \\ V_x \\ V_y \\ V_z \end{bmatrix}, \tag{4.14}$$

which is not a linear transform. R, r_x, r_y, and V_r, the parameters directly measured by the radar, are assumed to be corrupted by additive Gaussian noise, v_k. These measurements can be converted to Cartesian form directly to be in the same form of $\mathbf{x}$ in (4.1); however, this conversion causes the noise to be non-Gaussian [21].

For a random variable $\mathbf{z} = h(\mathbf{x})$ with a distribution $p(\mathbf{z})$, the distribution of $\mathbf{x}$ is given

$$p(\mathbf{x}) = |\mathbf{J}|^{-1} p(\mathbf{z}), \tag{4.15}$$

where $\mathbf{J}$ is the Jacobian matrix relating $h(\mathbf{x})$ to $\mathbf{x}$, as shown in equation 4.16 [21].

The Jacobian also serves as a first-order Taylor series expansion of $h(\mathbf{x}_k)$ about $\hat{\mathbf{x}}_k^-$, which is a way of linearizing (4.14) to the transform matrix H in (4.8) and (4.10).

$$\mathbf{H} = \mathbf{J} = \left.\frac{\partial h}{\partial \mathbf{x}}\right|_{\mathbf{x} = \hat{\mathbf{x}}_k^-} =$$

$$\begin{bmatrix}
\frac{1}{R} - \frac{x^2}{R^3} & -\frac{xy}{R^3} & -\frac{xz}{R^3} & 0 & 0 & 0 \\
-\frac{xy}{R^3} & \frac{1}{R} - \frac{y^2}{R^3} & -\frac{yz}{R^3} & 0 & 0 & 0 \\
\frac{x}{R} & \frac{y}{R} & \frac{z}{R} & 0 & 0 & 0 \\
\frac{V_x}{R} - \frac{xV_r}{R^2} & \frac{V_y}{R} - \frac{yV_r}{R^2} & \frac{V_z}{R} - \frac{zV_r}{R^2} & \frac{x}{R} & \frac{y}{R} & \frac{z}{R} \\
0 & 0 & 0 & 1 & 0 & 0 \\
0 & 0 & 0 & 0 & 1 & 0 \\
0 & 0 & 0 & 0 & 0 & 1
\end{bmatrix} \tag{4.16}$$

$^*R = \sqrt{x^2 + y^2 + z^2}$

Because the measurement vector $\mathbf{z}$ is in a different form than the state vector $\mathbf{x}$, the measurement covariance matrix $\mathbf{R}$ will also be different. A measurement's noise variance depends on the measurement's resolution and SNR. Range resolution is directly dependent on the signal's bandwidth. For a signal with a bandwidth β, M pulses per CPI, a pulse repetition frequency F_p, and N antennas transmitting in the x dimension, the resolutions are defined as follows:

$$\Delta R = c/2\beta \tag{4.17}$$

$$\Delta V_r = \lambda/2MF_p \tag{4.18}$$

$$\Delta r_x = 2/N_{tx} \tag{4.19}$$

$$\Delta r_y = 2/N_{ty} \tag{4.20}$$

The components of the target's velocity, $< V_x, V_y, V_z >$ are estimated to be equal to $\hat{\mathbf{V}}^- + \Delta v$, or some very small offset of the predicted velocity. The mea-

surement error variance matrix, R, is

$$\begin{bmatrix} \frac{\Delta r_x^{\,2}}{2SNR} & 0 & 0 & 0 & & & \\ 0 & \frac{\Delta r_y^{\,2}}{2SNR} & 0 & 0 & & & \\ 0 & 0 & \frac{\Delta R^{2}}{2SNR} & 0 & & \mathbf{0} & \\ 0 & 0 & 0 & \frac{\Delta V_r^{\,2}}{2SNR} & & & \\ & & & & \hat{\mathbf{P}}^{-}_{k\,4,4} & \cdots & \hat{\mathbf{P}}^{-}_{k\,4,6} \\ & & \mathbf{0} & & \vdots & \ddots & \vdots \\ & & & & \hat{\mathbf{P}}^{-}_{k\,6,4} & \cdots & \hat{\mathbf{P}}^{-}_{k\,6,6} \end{bmatrix}. \tag{4.21}$$

The terms $\hat{\mathbf{P}}^{-}_{k\,4,4}$ through $\hat{\mathbf{P}}^{-}_{k\,6,6}$ are the variances and covariances of the terms in $\hat{\mathbf{V}}^{-}$, the a priori estimate of the target's velocity.

4.2 Estimate uncertainty

$\hat{\mathbf{P}}$ is a measure of the state estimate error covariance. $\hat{\mathbf{P}}^{+}_{0}$, the initial estimate covariance, will match the measurement error covariance on the first detection. The $\mathbf{P}$ matrix will become smaller over time if the radar measurements are accurate [17] [22]. For a strictly linear, one-to-one Kalman filter (i.e., the transform $\mathbf{H}$ is an identity matrix), (4.8) is equivalent becomes

$$\mathbf{K} = \frac{\hat{\mathbf{P}}^{+}_{k}}{\hat{\mathbf{P}}^{+}_{k} + \mathbf{R}_k}, \tag{4.22}$$

The Kalman gain $\mathbf{K}$ in this situation approaches the identity matrix as $\mathbf{R}$ approaches zero, or as the measurement confidence increases to a maximum. If $\mathbf{K} = \mathbf{I}$ and $\mathbf{z}_k$ is in the same form as $\mathbf{x}_k$, (4.9) becomes

$$\hat{\mathbf{x}}_k^+ = \hat{\mathbf{x}}_k^- + \mathbf{I}(\mathbf{z}_k - \hat{\mathbf{x}}_k^-) = \mathbf{z}_k, \tag{4.23}$$

meaning that the Kalman filter believes the radar measurement to be perfectly accurate.

In this case, (4.10) would become

$$\hat{\mathbf{P}}_k^+ = (\mathbf{I} - \mathbf{I})\hat{\mathbf{P}}_k^- = \mathbf{0}. \tag{4.24}$$

It is not possible in a real situation for the measurement error to be zero. However, the above discussion describes how $\mathbf{R}$ weighs the accuracy of the measurement versus the estimated accuracy of the predicted state vector.

Conversely, if the SNR of a measurement is extremely low, that measurement should not be strongly weighted. If the radar does not detect one of the targets it is currently trying to track, it assumes that the SNR is essentially zero, meaning that the R matrix approaches infinity. This causes the Kalman gain K to drop to zero. For a Kalman gain of zero, (4.9) and (4.10) become $\hat{\mathbf{x}}_k^+ = \hat{\mathbf{x}}_k^- + \mathbf{0}$ and $\hat{\mathbf{P}}_k^+ = (\mathbf{I} - \mathbf{0})\hat{\mathbf{P}}_k^-$, respectively. If a measurement is poor or the radar fails to measure a track during a CPI, the state and covariance estimates are not updated. Multiple consecutive missed updates result in a gradual increase in uncertainty that will be further discussed in Chapter 6.

Chapter 5

Digital Array Division

All-digital arrays have a transmit-receive element on every antenna, meaning that every radiating element can produce a unique waveform. Each element can also apply a phase shift on its transmitted signal to steer the transmit beam in a target's direction. When groups of adjacent elements transmit the same signal aimed at the same target, that target's SNR increases. This chapter describes the process by which an all-digital array can be divided into transmitting sub-arrays that contain just enough elements to detect their intended targets.

5.1 Resource Requirements

A target's post-processing SNR depends on the square of the number of transmitting antennas steered towards the target, as described in (2.22). To achieve a certain desired SNR, the radar needs to assign a sufficient number of antennas to point at each target.

As Figure 5.1 shows, each antenna in the array emits a signal that propagates straight outward. A steerable beam is formed by applying phase shifts between elements transmitting the same waveform. This means that multiple antennas must

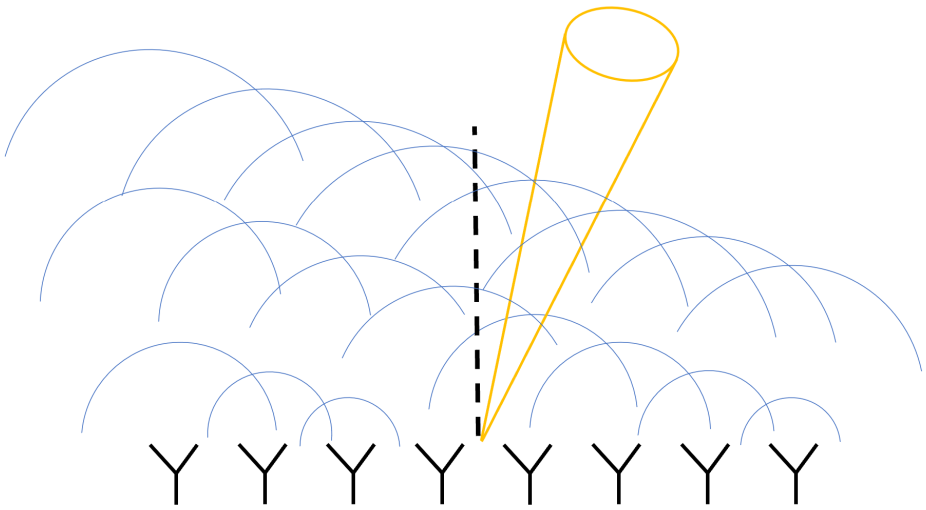

Figure 5.1: Representation of Phased Array Beam Steering

transmit the same waveform for steering to be possible. Some systems may have physical and software limitations on the smallest possible sub-array, called a minimum array unit (MAU) [6].

For the radar simulated in this thesis, let L be the side length of the square containing the minimum number of MAUs to theoretically give a target an SNR above a desired threshold (T) according to

$$L = \left\lceil \sqrt{\left\lceil \sqrt{T/SNR_1}/16 \right\rceil} \right\rceil, \tag{5.1}$$

where SNR_1 is the theoretical target SNR if the transmitting sub-array consisted of a single element. For the purposes of this thesis, an MAU consists of a 4x4 square

array of antenna elements. Therefore

$$(16L^2)^2 SNR_1 \geq T; \tag{5.2}$$

a transmitting sub-array with L^2 antennas should provide at least enough SNR so that a target's received signal is visible over the noise floor.

5.2 Placement Algorithm

The phased-array radar system described in this thesis contains 1024 total elements or 64 MAU. The radar must determine how to arrange multiple sub-arrays within a 64 MAU square to aim at as many targets as possible during a CPI.

The problem of sub-array placement is a subset of widely researched problems in computer science known as a knapsack problem [23]. The general knapsack problem involves a number of objects with varying weights and some manner of boundary or limiting factor. In this case, the objects "weights" are the minimum array unit requirements. The limiting factor is that all sub-arrays must fit in an 8x8 square of MAUs. Specifically, this problem can be seen as a form of bin packing problem where each row of sub-arrays can be treated as a bin with a maximum capacity of 8 [23–25].

The algorithm shown in Figure 5.2 is a modified version of the First-Fit algorithm [24]. The First-Fit algorithm takes a list of objects sorted in decreasing size order. The algorithm places these objects in the first available spot in any existing bin, as shown in Figures 5.3 and 5.4. If there is not enough room in any existing

bin, a new bin is created.

The algorithm described in this thesis also checks to see if there is enough space below a sub-array that was previously placed. The general "First Fit" equation does not attempt to fit smaller items below other items already in a bin. Our sub-array assignment algorithm implements this check to attempt to fit as many sub-arrays as possible into an 8 X 8 square of MAU.

The following example demonstrated in Figures 5.3-5.8 shows the implementation of the sub-array packing algorithm on the set of targets in Table 5.1. Each target in the table requires a certain number of antennas to achieve an SNR at or above a specific threshold.

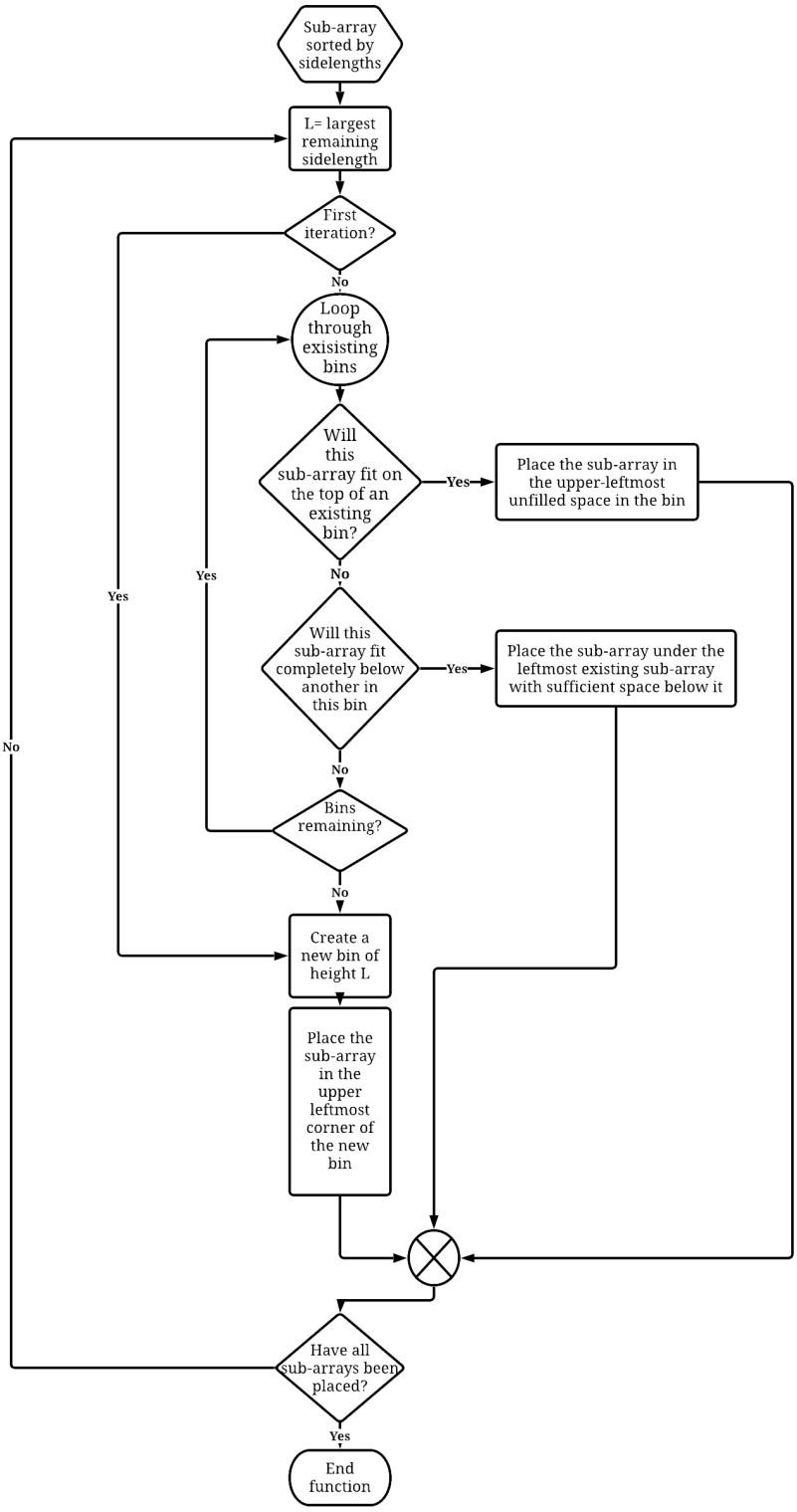

Figure 5.2: Sub-array Assignment Logic Tree

Target	Minimum Number of Antennas	L
1	120	3
2	100	3
3	80	3
4	64	2
5	61	2
6	57	2
7	48	2
8	32	2
9	32	2
10	25	2
11	12	1

Table 5.1: Example list of antenna requirements and sub-array sizes

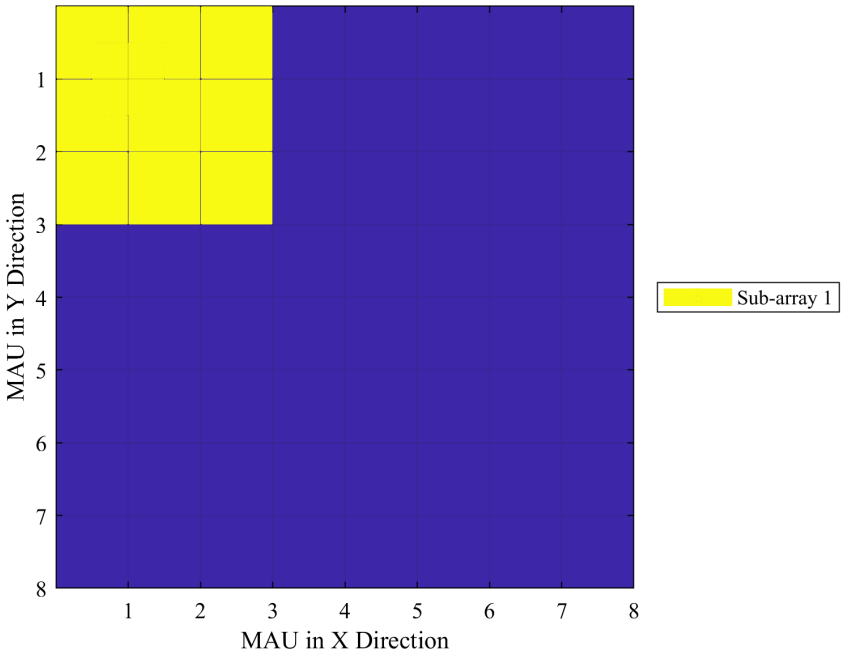

Figure 5.3: Placement of first sub-array

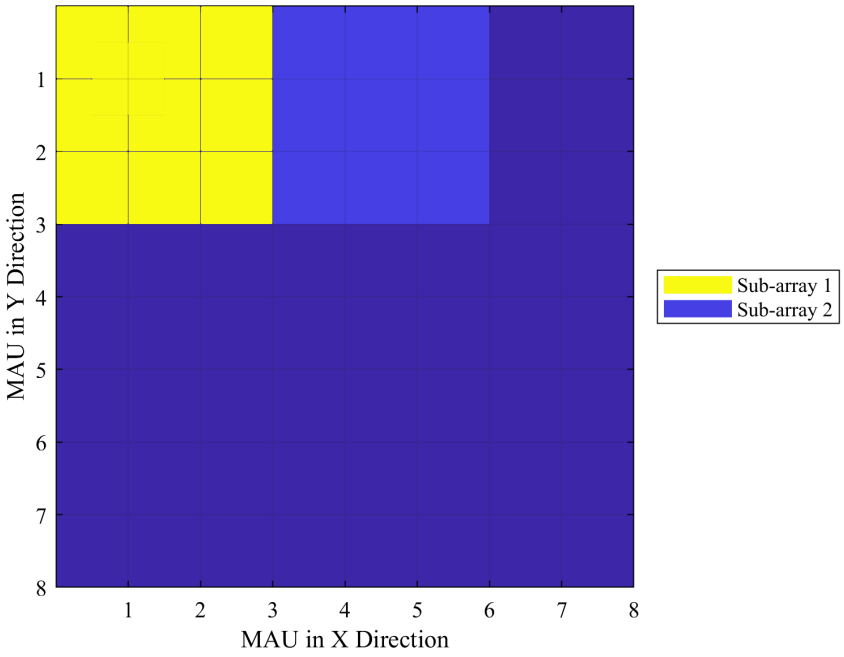

Figure 5.4: Placement of second sub-array

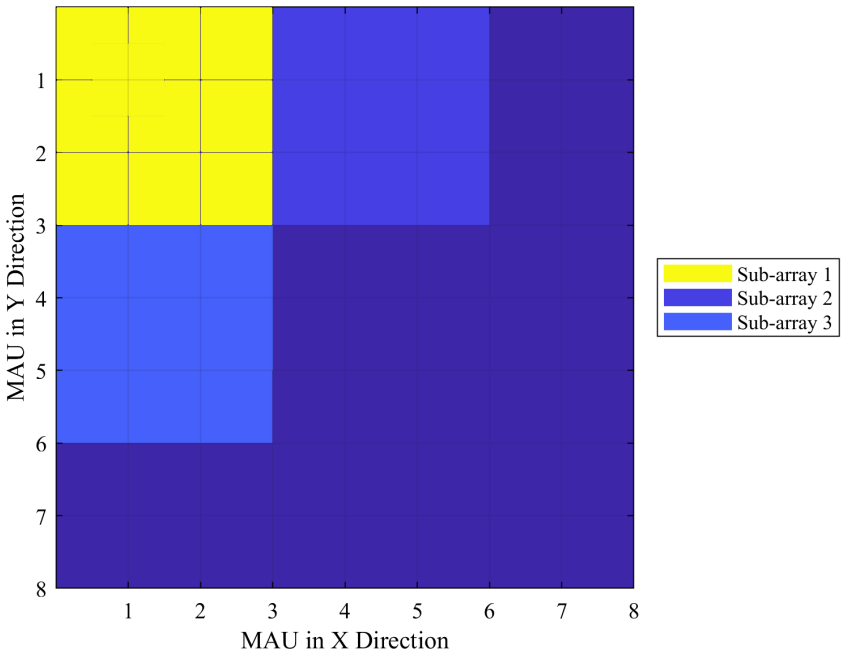

Figure 5.5: Creation of a new bin

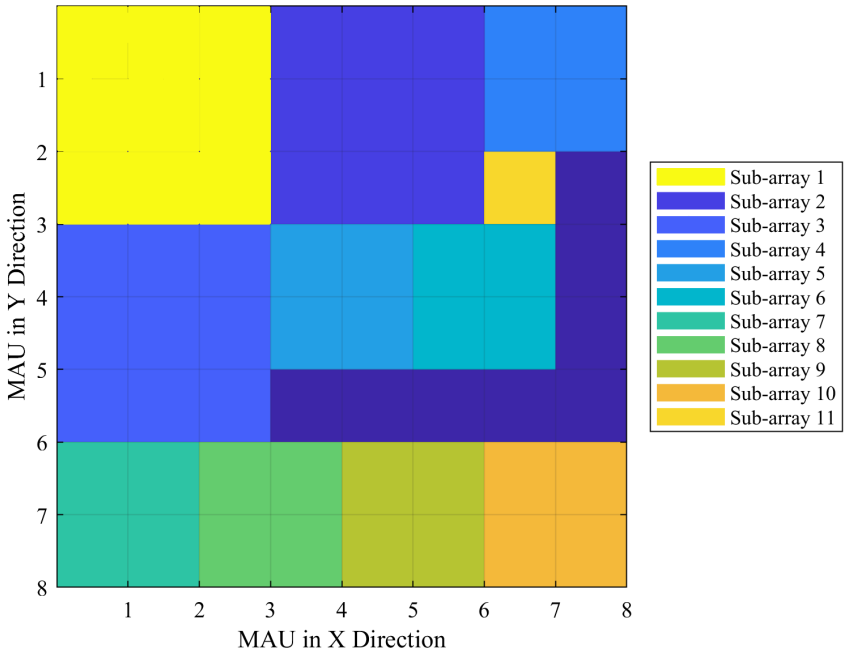

Figure 5.6: Packing one sub-array under another in the top bin

The final result of the sub-array packing algorithm is shown in 5.6. However, there is still some unused space in the antenna array. In order to optimize the use of resources, each MAU should be assigned to some target. If a bin is over half-full, that bin is horizontally extended to have a length of 8 MAU, as shown in figure 5.7. Any remaining empty space is assigned to the sub-array above it, as shown in figure 5.8. These rules are not specific to the First-Fit algorithm; they are meant to ensure that the entire array is used on transmit.

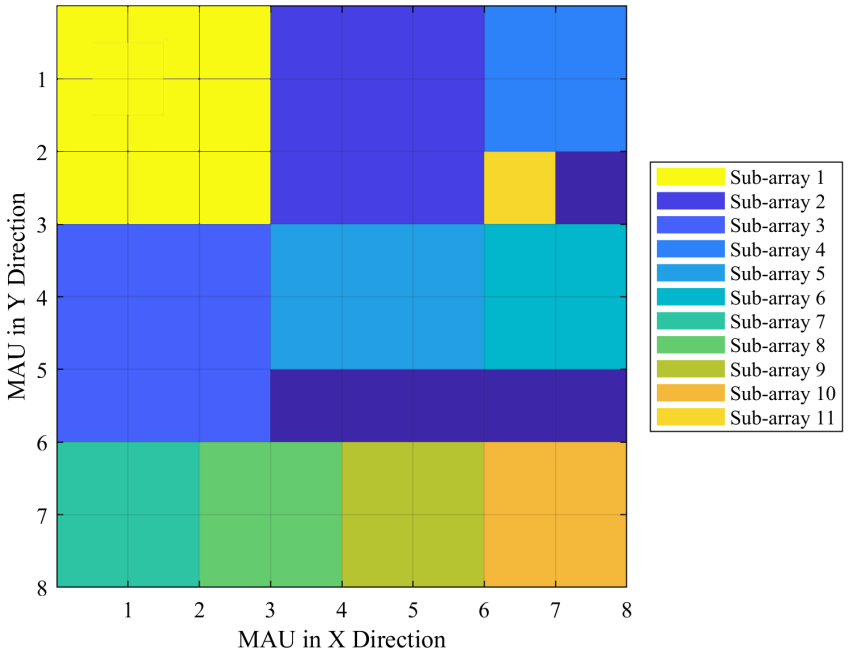

Figure 5.7: Array after bin-stretching

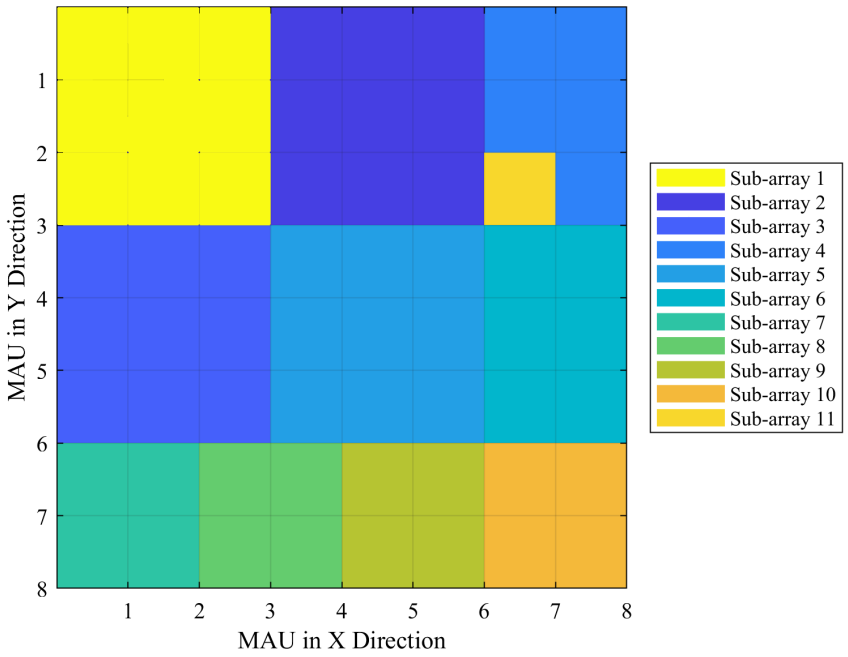

Figure 5.8: Filling remaining empty space

The 8x8 square in figure 5.8 is then extended to fit the whole 32x32 array of antennas. The worst-case scenario is that a sub-array will be L-shaped, causing a slightly irregularly shaped beam. This project assumes that there are no significant adverse effects on transmit beamforming based on L-shaped sub-arrays. The more antennas assigned to a sub-array, the finer the beam in r_x or r_y is. As table 5.2 shows, each of the sub-arrays in figure 5.8 has at least as many antennas as necessary to meet the required SNR threshold. In general, the algorithm assigns more antennas than the minimum.

The space-filling process can distort the sub-array sizes somewhat. Consider target 4 in this example. Sub-array 4 contains 5 MAUs or 80 antennas. Target 4 requires fewer than 80 antennas; however, sub-array 4 is not the 4th largest sub-array in Figure 5.8; sub-array 5 is. Because target 4 is weaker, it should have more transmitting elements than target 5. Therefore, the sub-arrays are assigned such that the targets with the greatest requirements correspond with the largest sub-arrays.

Target	Antenna Requirement	Corresponding Sub-Array	Assigned Antennas
1	120	1	144
2	100	2	144
3	80	3	144
4	64	5	144
5	61	6	96
6	57	4	80
7	48	7	64
8	32	8	64
9	32	9	64
10	25	10	64
11	12	11	16

Table 5.2: Array Division Algorithm Results

5.3 Transmit Beam Steering

The Kalman filter predicts a target's position and velocity, $\mathbf{x}_k$ for every CPI. The radar uses $\mathbf{x}_k$ to predict the unit vector between the radar and each target in order to aim transmit and receive beams in the targets' directions.

If multiple targets sit in the same direction, it is unnecessary to point more than one transmitting sub-array in that direction. The sub-array assignment algorithm first examines the predicted aiming vectors for each target. If the offset between multiple predicted aiming vectors is no more than $1/16$ in each direction (x, y, z),

the radar system assumes that the associated targets should be able to be detected by the same transmit beam. SNR_1 for that sub-array is equal to the lowest predicted SNR_1 value across each target.

SNR_1 is expected to show only small amounts of change between iterations. However, since a target's SNR in the radar equation is dependent on R^4; changes between the predicted and measured SNR_1 are taken into account. If a target's posterior range estimate for some CPI is R^+_{k-1} and the Kalman filter predicts that the target will be R^-_k meters away during the next CPI,

$$SNR^-_{1k} = SNR^+_{1k-1}(R^+_{k-1})^4/(R^-_k)^4. \tag{5.3}$$

5.4 Target Selection

For each CPI, the sub-array assignment algorithm determines all possible transmit beams and necessary sub-array sizes to aim at every target. There are some cases where the radar system will not have the capabilities or resources to update every target during every CPI. The sub-array assignment algorithm determines which possible sub-arrays take priority for placement in the actual 32 X 32 element array. In general, the radar should attempt to aim at the targets it is most likely to lose. The radar prioritizes aiming at targets that have the lowest number of detections.

Interference from other targets may prevent the radar from detecting some targets. A missed measurement happens when no detection corresponds with a target's predicted range and angle. This can only happen when a target explicitly has a transmitter beam pointed at it. When this happens, the target's a priori state estimate is

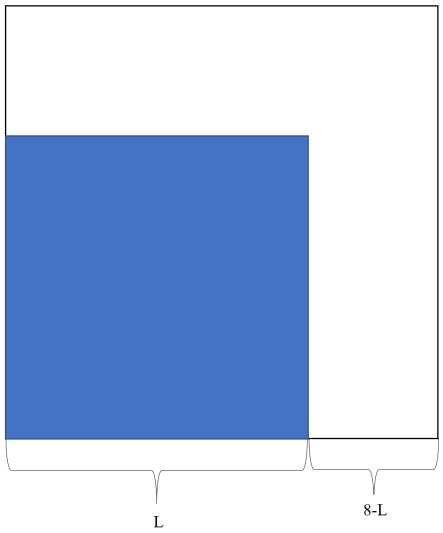

Figure 5.9: Possible sub-array configuration

not updated according to (4.8)-(4.10) because no valid measurement was made. If the radar continues to miss measurements on a specific target, it will lose track of that target. To avoid lost tracks, the radar prioritizes aiming at targets that were recently missed.

The sub-array assignment algorithm prioritizes sub-arrays that contain the most targets, especially those that have been recorded the fewest times. It also heavily weighs the number of consecutive CPIs in which a target has been missed, if applicable. The sub-array with the highest "necessity score" is chosen to be in the actual transmitting array. As figure 5.9 shows, if the highest weighted sub-array has a length L, the biggest square that can fit in the transmitting array has a size of $8 - L$. The sub-array with the highest necessity score will not necessarily have the greatest antenna requirement; antenna requirements are based on the target's distance from the radar system and RCS.

5.5 Abandoned Tracks

The radar system monitors when the receiver fails to detect a target. Although the target selection logic prioritizes lost tracks, there is a point where it is likely that the target reflection will not be strong enough for the radar to measure at all. If a target has not been detected for 3 consecutive CPIs where the radar has explicitly aimed at it, that target is considered lost. The array will stop tracking that target and save its resources for more visible targets.

The determinant of the state estimate error covariance, $\hat{\mathbf{P}}$, is a good estimate of the confidence in all estimates. $\mathbf{det}(\hat{\mathbf{P}})$ should be very large at the beginning of the tracking simulation. However, as the radar continues to accurately track a target, the value of $\mathbf{det}(\hat{\mathbf{P}})$ should decrease over time. Conversely, $\mathbf{det}(\hat{\mathbf{P}})$ will increase as long as a target is not being tracked, or if the estimated SNR is very low. If the value of $\mathbf{det}(\hat{\mathbf{P}})$ continues to rise during the tracker's steady-state operation, the associated target's SNR likely dropped enough so that it is no longer feasible to track.

Finally, if the number of MAUs needed to track a single target, calculated by L^2 in equation 5.1, is greater than 64, the target likely requires more resources than are available to the system. The radar will label that target as out of range and stop trying to track it.

Chapter 6

Minimum SNR Threshold and Update Frequency

This radar system detects a target based on the post-processed signal described in Chapter 3. The target should have a post-processing SNR of at least 15dB above the noise floor to be detected. The assumption that the post-processed radar signal is at least 15dB above the noise floor is a commonly used rule of thumb for reliable detection. As discussed in Section 2.2, a matched-filtered pseudorandom binary signal with a high value of $T_p\beta$ has sidelobes that are at least 15dB weaker than the mainlobe. A detection threshold of 15dB is high enough to avoid sidelobe detections but not so high that targets are ignored. If a target detection has a higher SNR, the controller becomes more confident in a given measurement.

(5.1) describes the number of antennas needed for a target's SNR to reach a certain threshold, T. T is a user-selected parameter; its value affects the system's behavior. A high value of T allows the measured targets to have higher SNR and therefore more confidence in the radar measurements. However, a high front-end threshold requires more antennas to reach it. This chapter examines the optimal front-end threshold that gives highly confident measurements without losing track of other targets due to infrequent measurements.

6.1 Simulation Setup

To determine the best value for T, the simulation was run on the same set of targets for $T = 13 - 28$. Each of the targets' paths remained well within the radar's unambiguous range. Each target also moved with a radial velocity that could be unambiguously measured by the target. For each CPI, the sub-array packing algorithm assigns at least as many elements so that the target SNR $\geq T$.

6.2 Estimate Uncertainty

Figure 6.1 shows an example of the determinant of the estimate error covariance $\hat{\mathbf{P}}_k^+$ over 15 seconds, or 300 CPIs, when $T = 13$dB. The initial estimate has a high level of error, significantly in the first half-second. Some of the targets' $\mathbf{det}(\hat{\mathbf{P}})$ values rise sharply and decay in a sort of sawtooth pattern. A sudden increase in $\mathbf{det}(\hat{\mathbf{P}})$ occurs when the radar fails to detect a target. This is because, according to (4.7),

$$\hat{\mathbf{P}}_k^- = \mathbf{F}\hat{\mathbf{P}}_{k-1}^+\mathbf{F}^T + \mathbf{Q}.$$

For a missed measurement, (4.10) reduces to $\hat{\mathbf{P}}_k^+ = \hat{\mathbf{P}}_k^-$. Because $\mathbf{Q}$ is a non-negative matrix, $\hat{\mathbf{P}}$ will continue to increase as a track is not updated. However, if the radar can update that track within a few CPIs, $\mathbf{det}(\hat{\mathbf{P}})$ decreases to a near exponential decay.

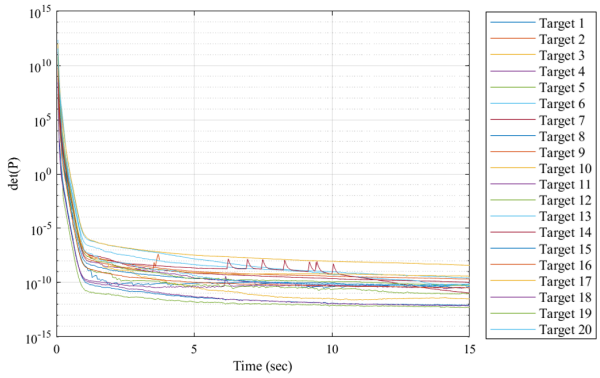

Figure 6.1: Estimate Uncertainty with $T = 13$dB

Figure 6.2 is a scatter plot of the SNR measurements of each target over the whole tracking interval. The target's SNR varies somewhat over time, but generally, a targets' SNR values stay within 5dB of one another.

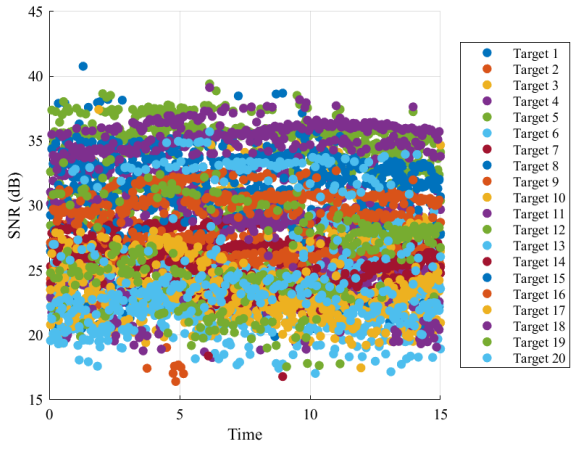

Figure 6.2: Target SNR with $T = 13$dB

Figure 6.3 is very similar to Figure 6.1 in structure; there are a few peaks where target measurements were missed, but the tracking algorithm generally was able to course-correct. During the steady-state operation, $\mathbf{det}(\hat{\mathbf{P}})$ is generally smooth, has a low value, and is very slowly decaying. This implies that the targets are still

being measured often and that the radar controller is very confident in those measurements.

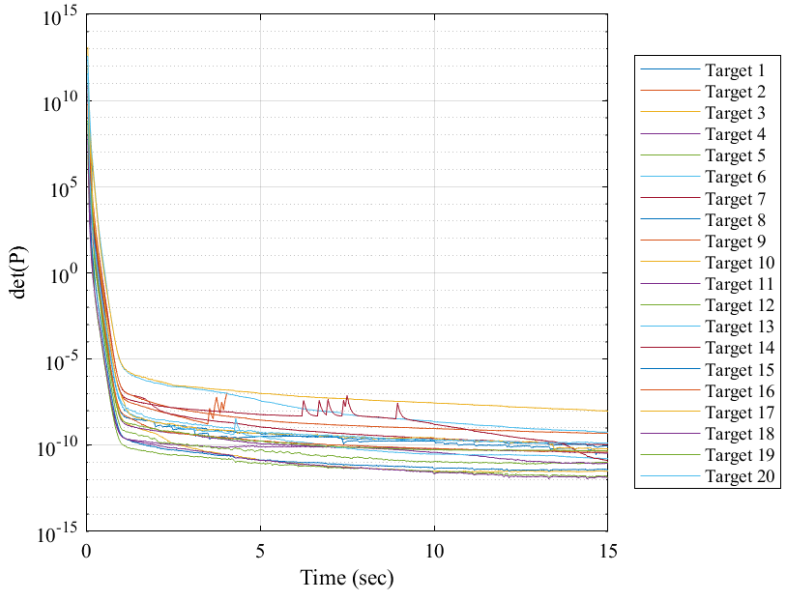

Figure 6.3: Estimate Uncertainty with $T = 15$dB

Figure 6.4 shows that the measured SNR for a front-end threshold of $T = 15$dB is nearly identical for the case where $T = 13$dB. This is because although the antenna requirement may increase, the sub-array packing algorithm usually assigns more antennas than necessary for each target to have an SNR of T. Any target measured by the sub-array will have at least 16 elements pointed at it. If the antenna requirement is higher, the next-smallest possible square of MAUs consists of 64 elements. The possible sub-array sizes before they are stretched to fit the entire array are $16N^2$ for $N = 1, 2, 3, ..., 8$. For similar values of T, targets' antenna requirements will often track to the same size sub-arrays.

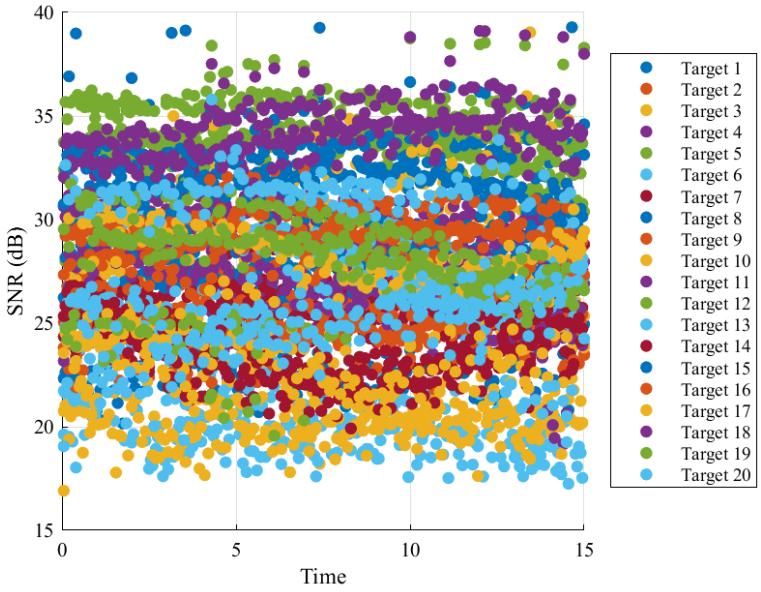

Figure 6.4: Target SNR with $T = 15$dB

According to Figure 6.5, when $T = 18$dB, missed measurements happen more often than when $T = 13$dB or 15dB. The decrease in update frequency happens because the transmitting element requirements are high enough that fewer sub-arrays can fit inside the MIMO array at once. A lower update frequency means causes the controller to lose confidence in its estimates over time. Figure 6.6 shows that increasing the front-end threshold from 15dB to 18dB does improve the measured SNR compared to smaller values of T.

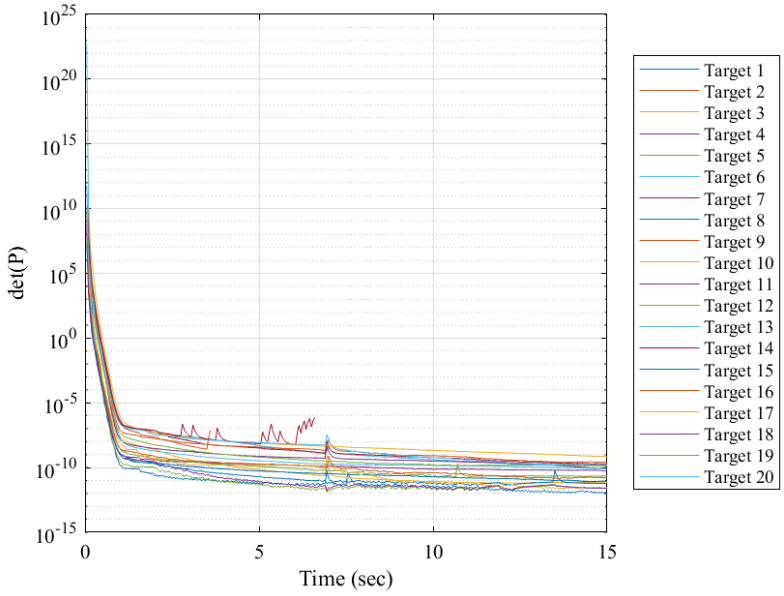

Figure 6.5: Estimate Uncertainty with $T = 18$dB

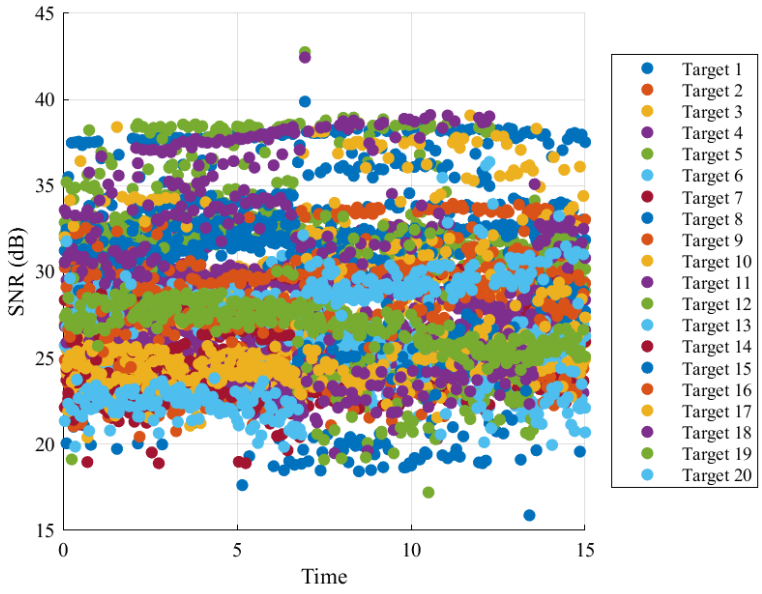

Figure 6.6: Target SNR with $T = 18$dB

When $T = 25$dB, Figure 6.7 shows that the plots of $\mathbf{det}(\hat{\mathbf{P}})$ look less like a smooth exponential decay over time. Because fewer sub-arrays that yield $T = 25$

can fit in the entire array, the targets are not being updated nearly as often as when $T = 15$. $\mathbf{P}$ increases sharply as tracks are not updated. However, as Figure 6.8 shows, the SNR of the targets' measurements is generally higher than when $T = 15$dB. This means that when the tracks are updated, the estimate confidence is higher and $\mathbf{det}(\hat{\mathbf{P}})$ is smaller. The measured SNR values are also more varied, which contributes to the fluctuations in estimate confidence.

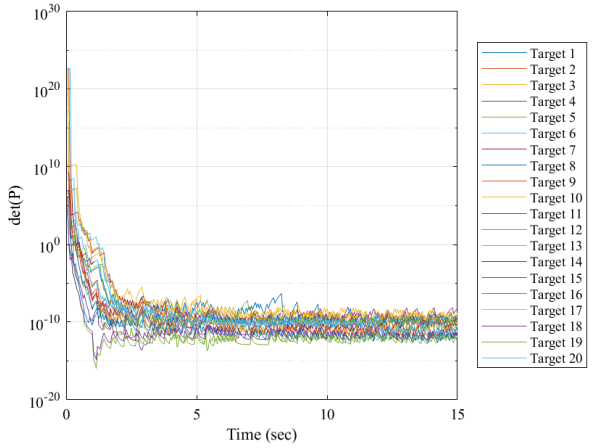

Figure 6.7: Estimate Uncertainty with $T = 25$dB

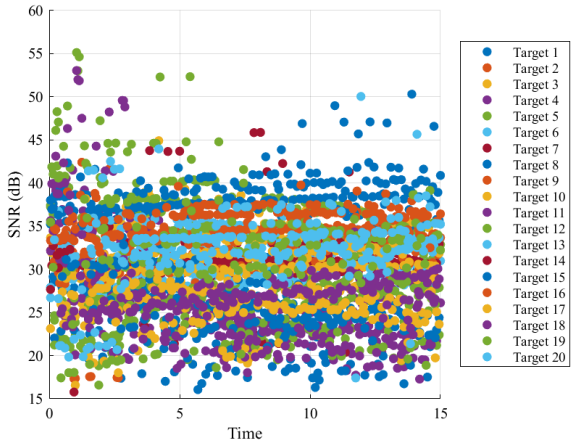

Figure 6.8: Target SNR with $T = 25$dB

Figures 6.9 and 6.10 show the same pattern; as T increases, the plots of $\mathbf{det}(\hat{\mathbf{P}})$ become rougher and the measured SNR values become generally higher but less consistent. $\mathbf{det}(\hat{\mathbf{P}})$ decays to a lower value as T increases.

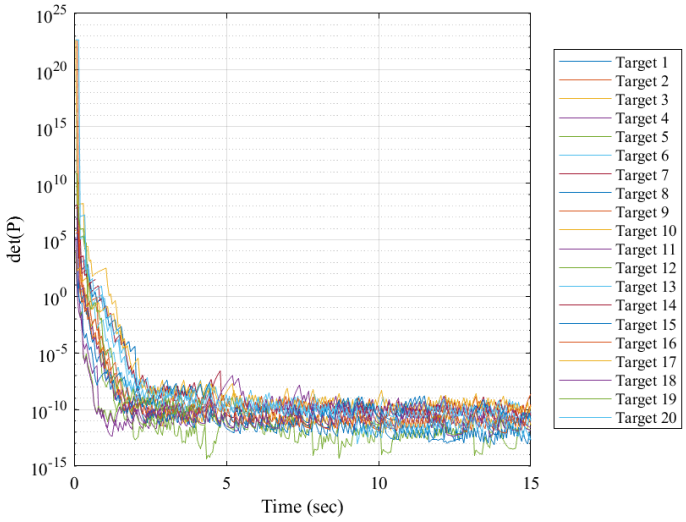

Figure 6.9: Estimate Uncertainty with $T = 28$dB

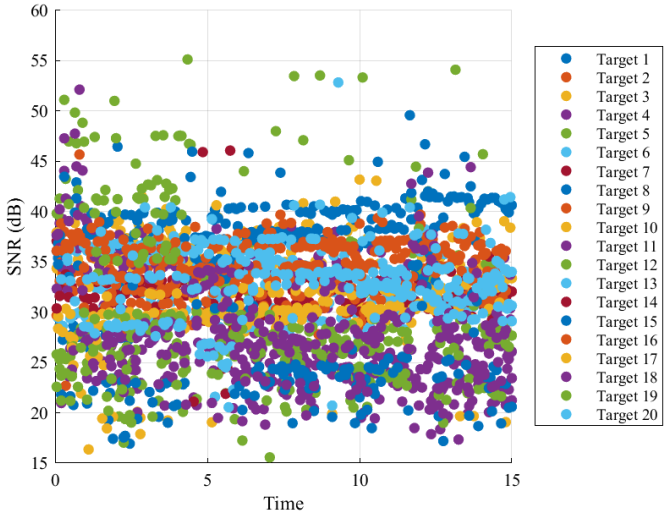

Figure 6.10: Target SNR with $T = 28$dB

6.3 Missed Measurements

In our simulated experiments, we specified that after 3 consecutive misses, the radar should stop tracking a specific target. For an all-digital phased array measuring multiple targets, there is a fundamental tradeoff between target SNR and update frequency. Larger transmitting sub-arrays improve target SNR. However, fewer large sub-arrays can fit inside a 32 x 32 element array, meaning the radar may not detect as many targets per CPI. T should be set at a threshold that is high enough to ensure strong target detections but not so high that the radar loses tracks due to low update frequency. Figures 6.11 - 6.17 show that the number of missed measurements increases as T increases.

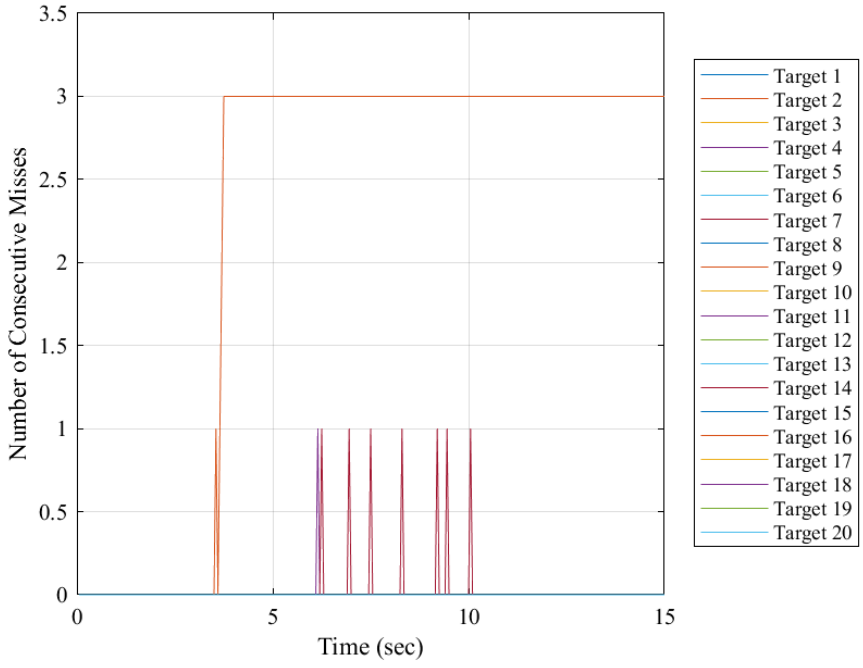

Figure 6.11: Missed Measurements with $T = 13$dB

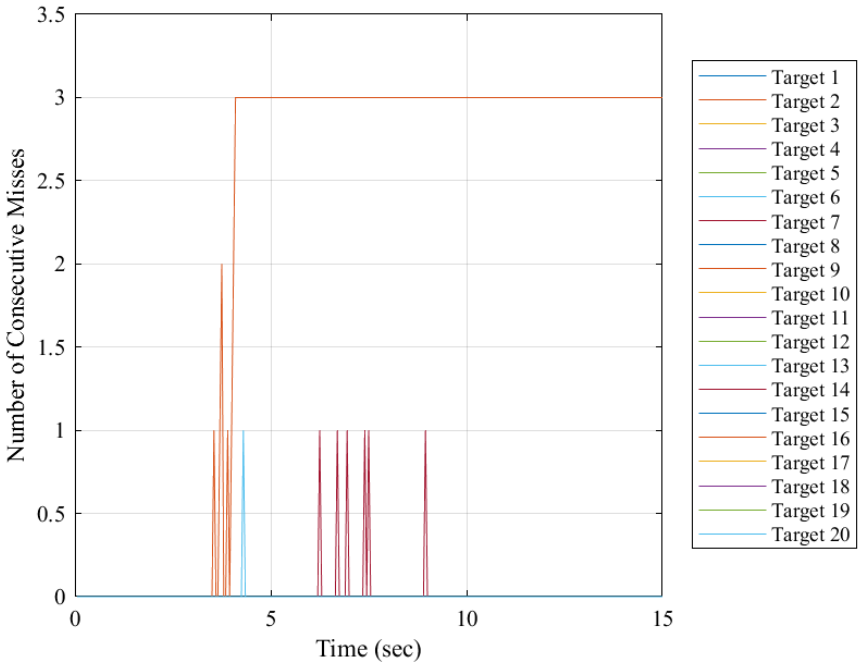

Figure 6.12: Missed Measurements with $T = 15$dB

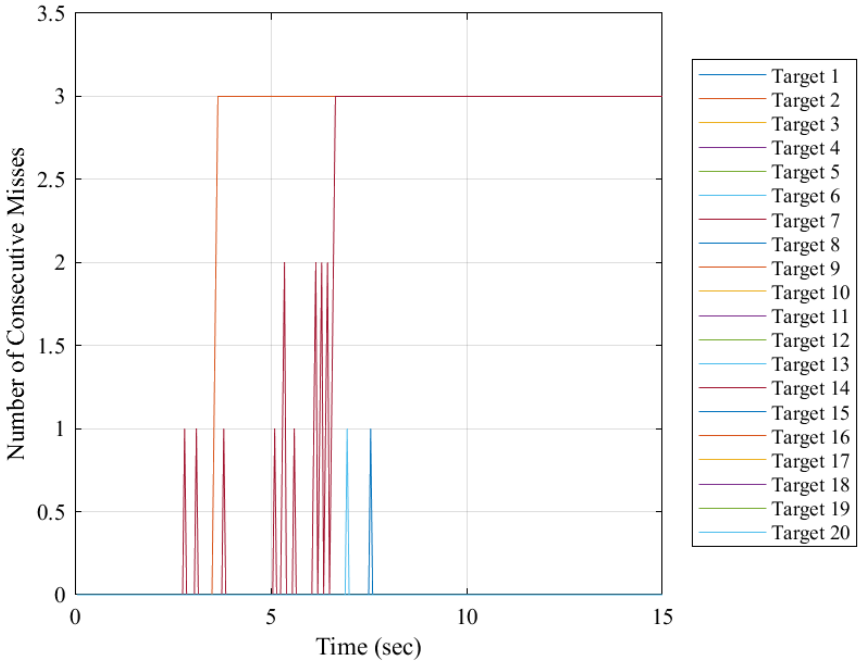

Figure 6.13: Missed Measurements with $T = 18$dB

In Figures 6.11 - 6.17, target 2 consistently gets lost within the first few seconds. At this point, target 2 is right next to target 4. As figures 6.14 and 6.15 show, these two targets are about 13 meters away from one another. The signal processor assumes that the weaker target is in the stronger target's sidelobes. Since the targets do not move much between subsequent CPIs, this issue happens three times in a row, causing the controller to assume it has lost target 2. This could potentially be dealt with by more sophisticated handling of sidelobe detection for large targets.

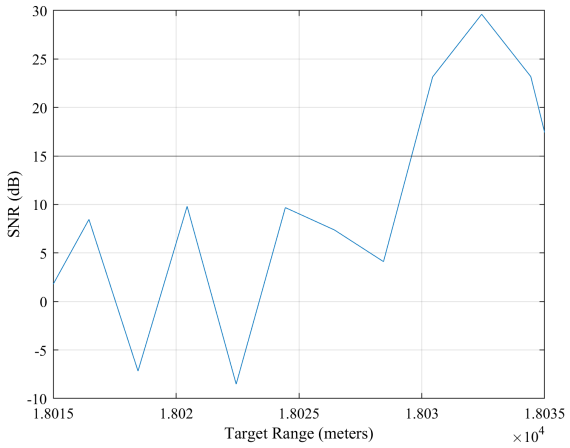

Figure 6.14: Target 4 Matched Filter Slice

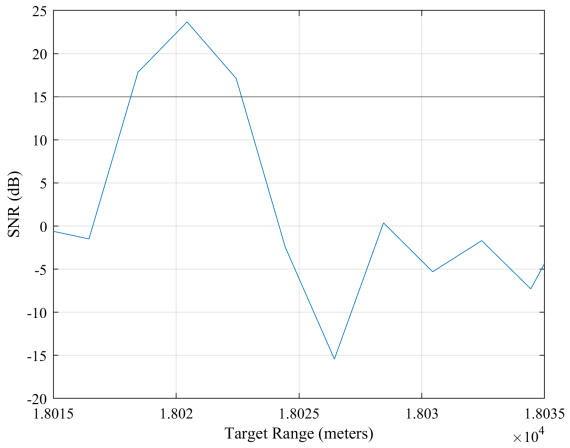

Figure 6.15: Target 2 Matched Filter Slice

To attempt to combat the effects of weaker targets being overshadowed by stronger crossing targets, a simulation was run where targets with similar aiming vectors were tracked by different sub-arrays. However, this method proved worse. Figure 6.16 shows the consecutive missed measurements when $T = 15$ and transmit beams were aimed at each target without grouping them together. Compared to figure 6.12, there are more misses. Crossing targets still appear in stronger targets' sidelobes. Because targets theoretically will not be sharing transmit beams, more transmitting sub-arrays are necessary to implement this method. Because more sub-arrays are required, update frequency suffers.

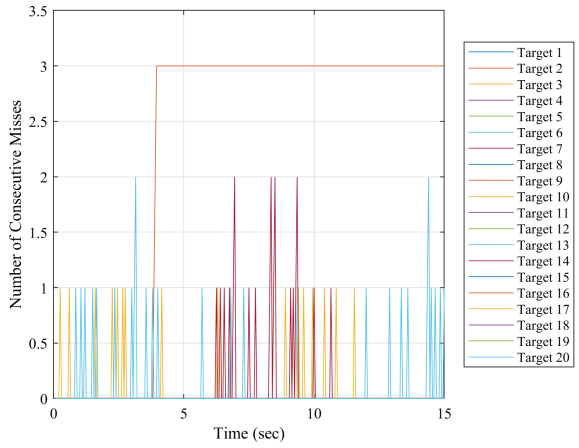

Figure 6.16: Missed Measurements Without Grouping

As the threshold T increases above 15dB, more and more targets are lost. Figure 6.17 shows that the radar completely abandons target 14 as well as target 2 when $T = 18$dB. Target 14 has several missed measurements as it is one of the weaker targets in this experiment. Eventually, the radar abandons target 14 in favor of targets it can more reliably detect.

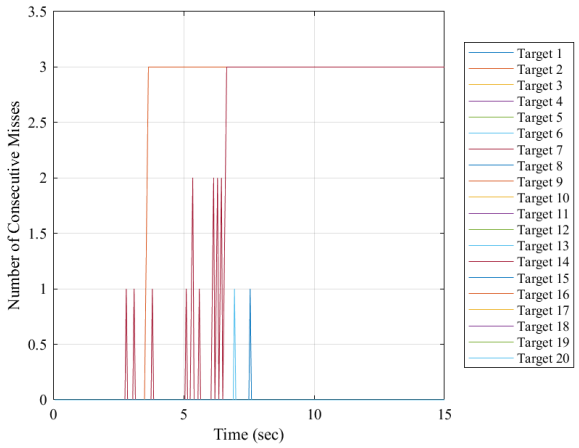

Figure 6.17: Missed Measurements with $T = 18$

When $T = 28$dB, radar misses occur more frequently. In most cases, the radar is able to update a target after a measurement is missed. However, the radar still has to abandon a third target because its detection frequency is not high enough to keep track of weaker targets.

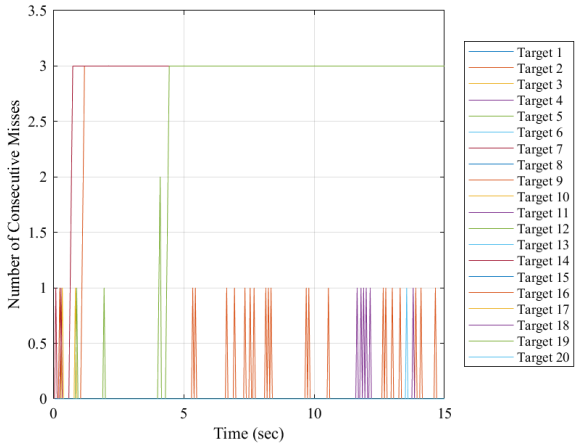

Figure 6.18: Missed Measurements with $T = 28$

6.4 Alternate Method

The best possible SNR that a target measured by an antenna array can achieve occurs when the whole array is used to measure it. Because there are 1024 antennas in our simulated array, the gain is $\log_{10}(1024^2) \approx 60$dB better than that of a single radiating antenna. Dividing the array into multiple sub-arrays sacrifices some of this gain, meaning that there is less confidence in any given radar measurement.

As a comparison, the performance of a phased array that does not divide the sub-array was tested. This array pointed at a single target every CPI. For example, if there are 10 targets within the radar's field of view and the simulation is running for 300 CPIs, the array should aim at each target 30 times. Theoretically, the SNR and, therefore, the individual measurement confidence should be higher than that of the sub-array division method. However, each target will be measured fewer times overall.

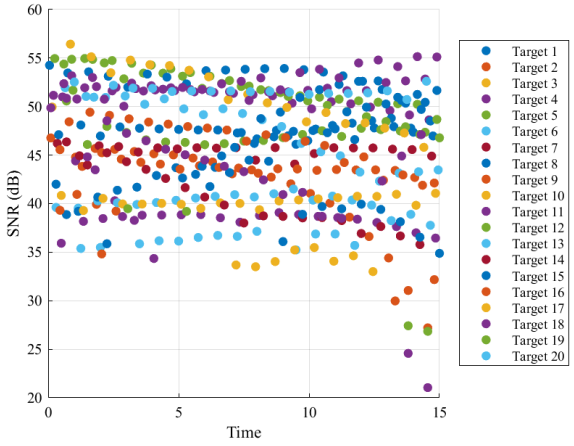

Figure 6.19: Target SNR Without Array Division

Figure 6.19 shows that, when all 1024 targets point at each target, each target's

SNR is much higher than when the array is sub-divided to point at many targets. However, measurement frequency is much lower with this method.

In Section 5.5, the radar chooses to abandon tracks if $\mathbf{det}(\hat{\mathbf{P}})$ increases greatly during the tracker's steady-state operation. This criterion causes the controller to abandon several of the tracks in the first few seconds, as shown in Figure 6.21. The estimate uncertainty has a sawtooth pattern instead of a strictly smooth exponential decay; the error covariance decreases with every measurement, then steadily increases until another measurement is made.

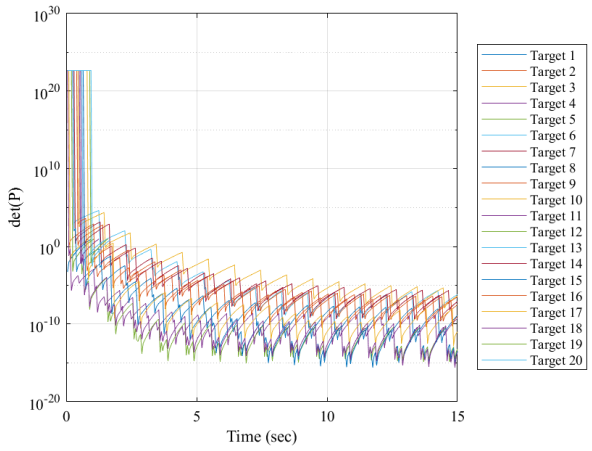

Figure 6.20: Estimate Uncertainty Without Array Division

Figure 6.21 shows that the radar is unable to course-correct after a single miss when the array is not sub-divided. This happens because, if a target is missed, the algorithm no longer prioritizes re-gaining a missed track. The radar attempts to find that target after 20 more CPIs but is unable to do so.

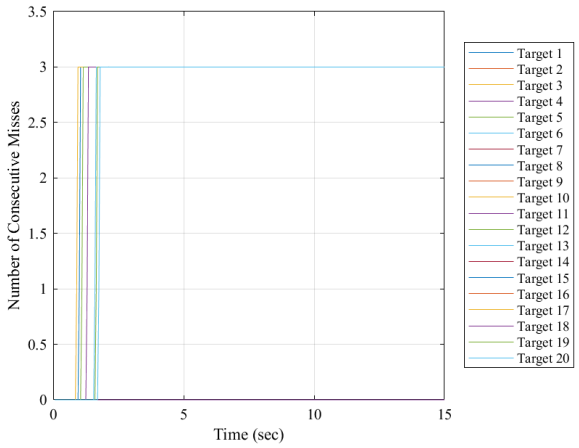

Figure 6.21: Missed Measurements Without Array Division

6.5 Update Frequency

For the purposes of this study, a detection is defined as when a target, whether explicitly aimed at or not, is measured at (or very near) its true location. Figure 6.22 shows several box-and-whisker plots that describe the number of target detections over the course of 300 CPIs based on the minimum SNR threshold T. The "+" signs indicate statistical outliers on the box and whisker plots; these low range outliers indicate when one of the 20 targets was lost early on during the tracking period. Table 6.1 contains information about the number of tracks maintained throughout the entire tracking period, as well as the median number of detections for each target. From $T = 13 - 15$dB, most of the targets are detected during nearly every CPI. At $T = 16$dB, another target is lost about halfway through the simulation run. The mean number of detections drops as T increases. As the minimum SNR threshold increases, the array division algorithm assigns more antenna elements to each target; the array is, therefore, unable to detect as many targets. The overall number of target detections decreases as the antenna requirement increases.

In the case where the full array is used on transmit, no target is measured more than 100 times. Many targets are lost after a single detection. This is because the radar is not confident in the position estimates and devotes its resources to targets that have higher degrees of confidence.

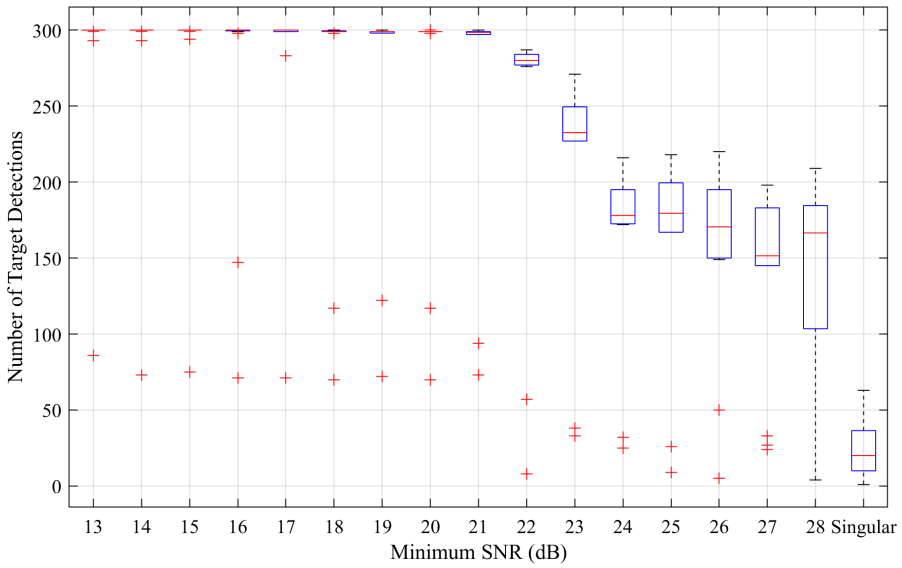

Figure 6.22: Target Detections vs Minimum SNR

6.6 Conclusion

Dividing a MIMO antenna array into sub-arrays using the methods described earlier in this paper is very effective at tracking multiple targets. It outperforms an undivided array system; a divided array gives more certain measurements and does not lose as many tracks. For a target to be detected above the noise threshold, its post-processing SNR should be at least 15dB. Equation 5.1 determines the minimum number of transmitting antennas to reach some threshold T. In our case, one

Minimum SNR (dB)	Tracks Maintained	Median Target Detections
13	19	300
15	19	300
17	19	300
18	18	299
20	18	299
22	18	280
24	18	178
26	18	170.5
28	15	166.5
Singular	15	20

Table 6.1: 20 Target MIMO Radar Predictive Tracking Results

MAU consists of 16 antennas, and any sub-array must have at least $16L^2$ antennas, which will almost always exceed the actual minimum number of transmitting antennas needed to achieve an SNR of 15dB. Because the actual number of transmitting antennas will exceed the minimum in most cases, setting a front-end threshold slightly smaller than 15dB will generally be sufficient.

When the SNR threshold is set higher, the measurement confidence may be stronger. However, setting too high of a front-end threshold may cause some targets' SNRs to overshadow nearby targets. It also decreases the update frequency, which decreases the controller's confidence in the state estimate. A front-end threshold of $T = 15$dB allows for a high degree of measurement confidence without over-allocating antennas and sacrificing update frequency.

Chapter 7

Comparisons for Large Target Count

As Chapter 6 shows, the system is able to track 20 targets fairly easily with a front-end threshold of 15dB. As the number of targets increases but the front-end threshold stays the same, targets may not be updated as often. In this section, the simulation was run on data sets with an increasing number of targets. Additionally, these targets were generated so that no two targets are in the same spatial frequency resolution. This eliminates the issue of crossing targets and ensures that when a target is lost, it is because the radar lacks sufficient resources to track it properly.

The figures in this section do not have legends, as the different colored lines correspond to the number of targets. As the number of targets increases, it becomes less important to examine the behavior of individual targets and more important to focus on the overall trends.

For a randomly generated set of 10 targets, the simulation was able to assign at least enough antennas to aim at every target over the whole CPI. Because each target was measured every CPI and no two targets could exist in the same transmit beam, the sub-array sizes stayed constant throughout the whole tracking period. Figure 7.1 shows the uncertainty in the targets' state vectors, which quickly converges to

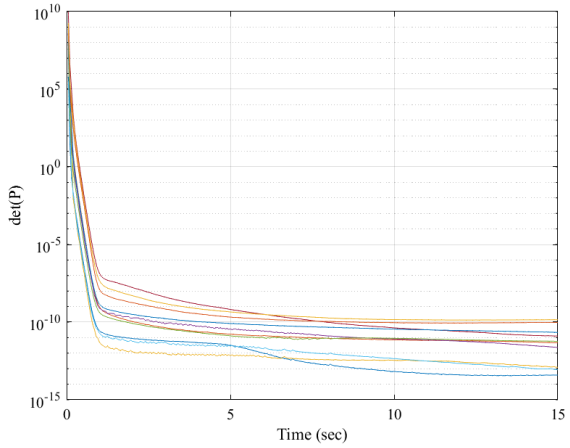

Figure 7.1: Cumulative Track Estimate Uncertainty for 10 Targets

near zero.

In our simulation setup, each element has a transmitting power of 10w. Each target is between 10 and 20 km away from the radar system. For the purposes of this study, each target's RCS remains constant across all CPIs; the RCS value for each target is an exponential random variable with a mean of $10m^2$. Under these conditions, the phased array can generally aim at around 10-15 targets per CPI. As the number of targets increases, the radar must decide which targets to ignore and which ones it should attempt to measure. Figure 7.2 shows the instances where the radar missed measurements for certain targets. The controller was generally able to course-correct and re-capture a target after it was missed.

The targets that were missed most frequently had very low RCS values, with one exception. One abandoned target had a strong RCS value, but its measured SNR value was not constant, as shown in figure 7.3. This was caused by the array assigning too many transmitting antennas to that target during one CPI, as shown

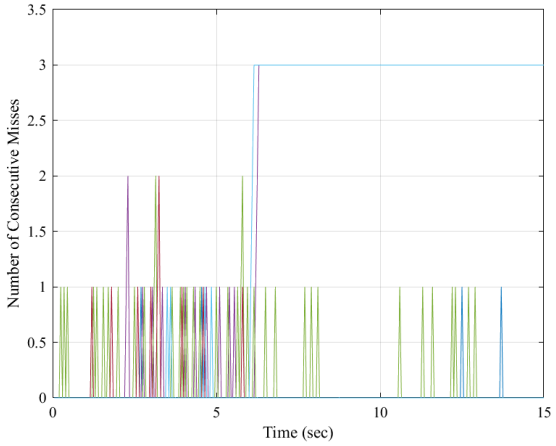

Figure 7.2: Missed Measurements with 20 targets

in 7.4, causing the target's SNR to surge. The array then used the inflated value of SNR to allocate resources in future CPIs. The spikes in that target's SNR caused the controller to overestimate its actual strength, eventually assigning it too few antennas for it to be properly measured.

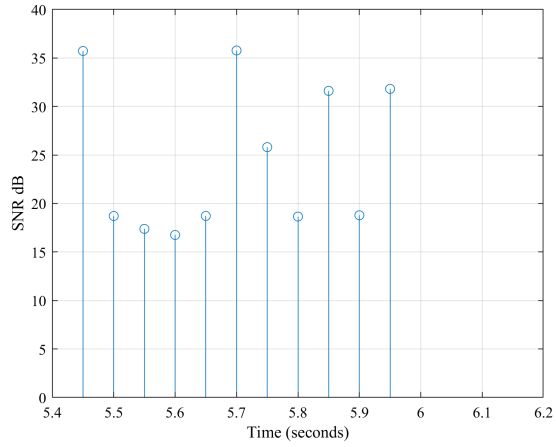

Figure 7.3: Oscillating values of Target SNR

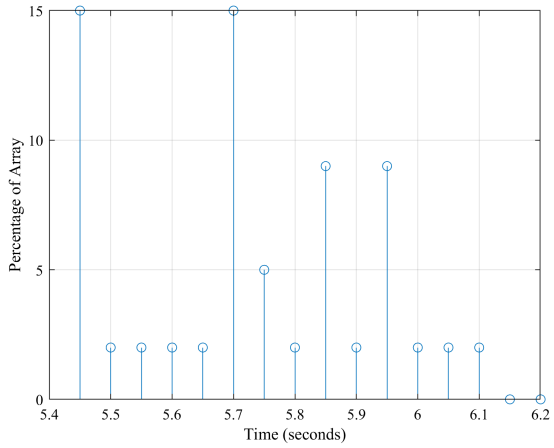

Figure 7.4: Percentage of transmit array assigned to a target

Figure 7.5 shows the determinant of $\hat{P}$ for the set of 20 target tracks. There are occasional spikes where the targets are lost for a few measurements, but the overall estimate confidence remains high.

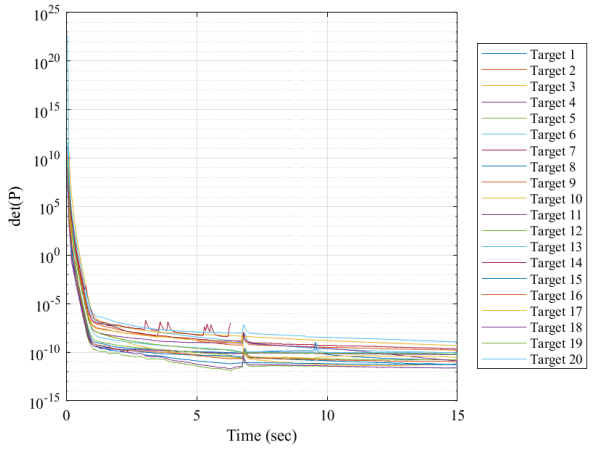

Figure 7.5: Cumulative Track Estimate Uncertainty for 20 Targets

Figures 7.6 and 7.7 show the radar system's behavior as it attempts to track 30 targets at once. The radar misses measurements fairly often, but it is generally able to update tracks after one or two consecutive misses. The radar does lose a few of

its weaker targets.

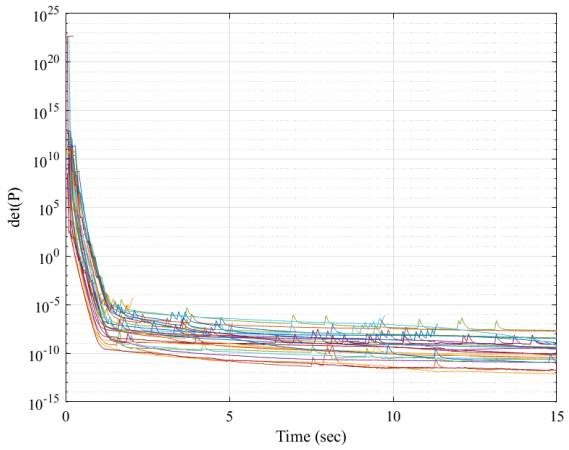

Figure 7.6: Cumulative Track Estimate Uncertainty for 30 Targets

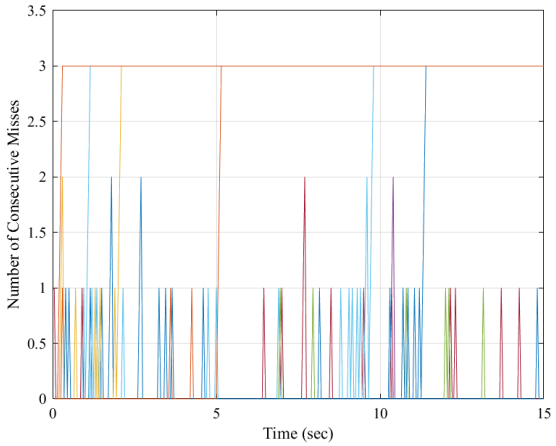

Figure 7.7: Missed Measurements with 30 Targets

The radar is still able to course correct after most missed measurements when tracking 40 targets simultaneously, as shown in Figures 7.8 and 7.9. However, because there are more targets to update in this experiment, the overall update frequency lowers. This causes $\mathbf{det}(\hat{\mathbf{P}})$ to converge more slowly.

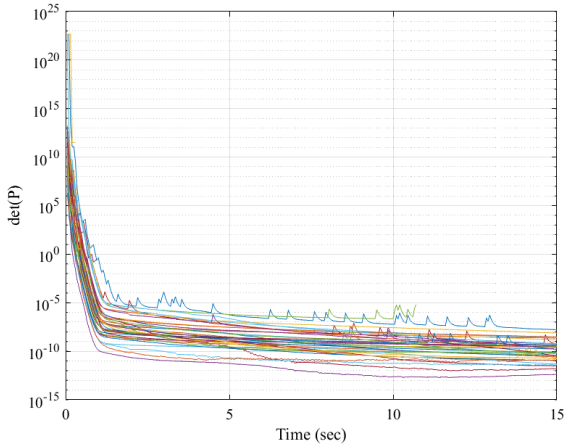

Figure 7.8: Cumulative Track Estimate Uncertainty for 40 Targets

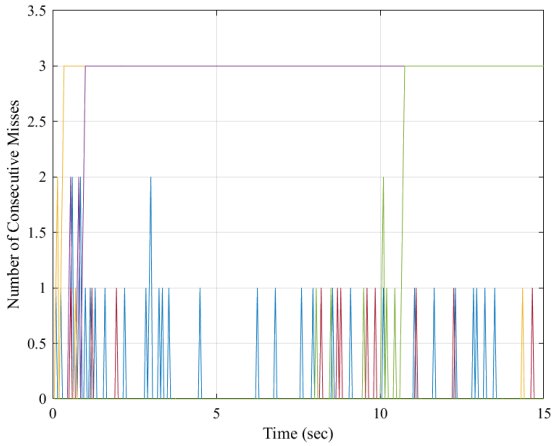

Figure 7.9: Missed Measurements with 40 Targets

This pattern continues when the radar attempts to track 50 targets at the same time. For some targets, the $\mathbf{det}(\hat{\mathbf{P}})$ plots are very smooth. Weaker and more uncertain targets' $\mathbf{det}(\hat{\mathbf{P}})$ values fluctuate over time.

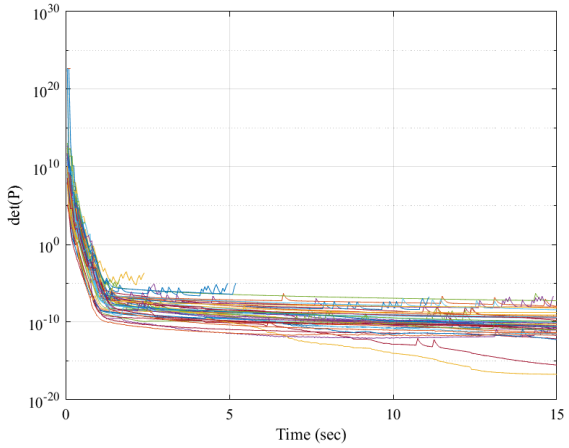

Figure 7.10: Cumulative Track Estimate Uncertainty for 50 Targets

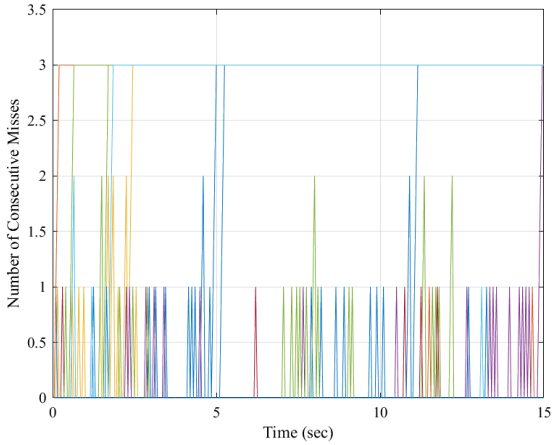

Figure 7.11: Missed Measurements with 50 Targets

The radar is still able to maintain many tracks as it attempts to track 100 targets at once, as shown in figure 7.12. The phased array can detect around 10 targets per CPI; when trying to track 100 targets, the update frequency drops drastically. Most of the $\mathbf{det}(\hat{\mathbf{P}})$ plots exhibit the sawtooth that indicates when tracks are not updated often. As figure 7.13 shows, the radar is still able to track targets even after a few consecutive misses. Although the MIMO radar system's performance decreases as it attempts to track more targets, the system is still able to update most targets often

enough to maintain several tracks.

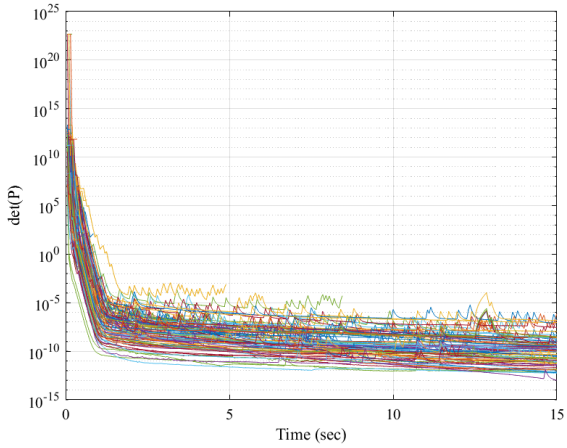

Figure 7.12: Cumulative Track Estimate Uncertainty for 100 Targets

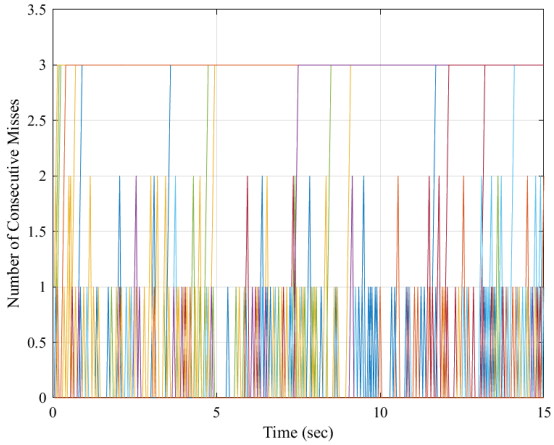

Figure 7.13: Missed Measurements with 100 Targets

7.0.1 Comparison with Sequential Array Method

The sequential array method described in Section 6.4 did not track 20 targets as efficiently as the divided-array method did. As a comparison, the sequential array method was run on the same set of 100 targets as in Figures 7.12 and 7.13. Figure 7.14 shows that, when the array attempts to aim at 100 targets sequentially,

the estimate confidence is very low because $\mathbf{det}(\hat{mathbfP})$ is very high. As table 7.1 shows, the tracker abandons 54 targets over the tracking period. The median number of detections for each target is 2.5 because the radar only aims explicitly at each target 3 times over 300 CPIs. Sub-divided radars have better performance when tracking many targets within a range.

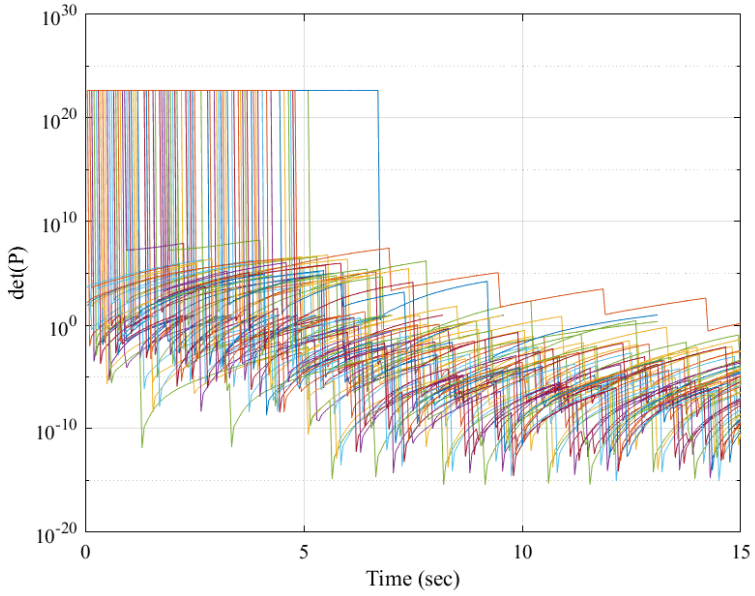

Figure 7.14: Cumulative Track Estimate Uncertainty for 100 Targets Without Array Division

7.1 Results

This chapter demonstrated an all-digital array's predictive tracking performance as it attempted to track many targets. The results of these experiments are shown in Table 7.1. The radar is able to track maintains at least 80% of the targets within a range of 10-20km. When the array is not sub-divided, the tracker loses more than half of the targets. Although the controller is unable to allocate sufficient resources for each target every CPI, the radar is generally able to update targets after missed

Number of Targets	Tracks Maintained	Median of Target Detections
10	10	300
20	18	295
30	24	290
40	37	298
50	41	293
100	84	290
100 (Sequential)	46	2.5

Table 7.1: MIMO Radar Predictive Tracking Results

measurements. However, because the radar system considers a track to be lost after three consecutive misses, weak or crossing targets are often rejected as the radar focuses its limited resources on the targets it consistently measures.

A possible way to improve the radar's performance is to increase the transmitting power. If P_t increases, the radar may assign fewer MAU to each target. However, the absolute maximum number of targets that can be aimed at per CPI is 64.

Chapter 8

Conclusions

This study overviews the fundamental operation of an all-digital multiple-input, multiple-output (MIMO) phased array. It describes pseudorandom biphase-coded waveforms, a set of waveforms that have a low peak-sidelobe-level and are relatively easy to generate, diverse, and weakly-cross-correlated. This thesis describes a simulation of a radar signal processor that is able to detect a large number of targets simultaneously.

This thesis also describes the decision-making process of the radar's controller: how it allocates resources to each target and how it predicts target movement over time. The radar measures spatial frequencies $\hat{r}_x$ and $\hat{r}_y$, as well as range and radial velocity. The actual velocity vector cannot be determined by this set of measurements. Each of these measurements is based on a discretized signal, so their values may lie within some range based on the radar's resolution. The controller predicts target motion based on SNR and measurement uncertainty.

Sub-divided all-digital arrays allow for the tracking of many more targets than traditional radar systems. The detection rate of this system is much higher than that of a radar that points at a single target for each CPI. As the number of targets

increases, the radar favors measuring most of the strong targets and occasionally abandons targets if their SNR values are too low.

8.1 Future Work

Although this thesis gives a strong implementation of an all-digital radar simulation, there is still room for improvement. The radar simulation assumes that each target's RCS does not change between CPIs; RCS values tend to change over the course of a real target's motion. Because SNR depends on a target's RCS, the controller would have to take RCS into account when allocating antenna elements to each sub-array. Future studies could use more realistic target models and possibly predict changes in RCS.

This thesis focused solely on tracking and ignored problems related to calibration and association. The simulated radar was able to determine the peaks in the post-processed range-Doppler-angle maps that corresponded to each target's actual position and velocity. In a real radar system, the issue of determining which detection is tied to which target is much more difficult. Radar detectors must determine the likelihood that a detection corresponds to a certain target based on how far each detection is from the tracker's a priori predictions. The problem of detection association is extremely complex, especially in the cases where targets cross in front of one another [26]. Implementing some manner of statistical target association is a very logical next step for the study of all-digital radar.

In Chapter 6, many of the minimum SNR requirements mapped to similar

results. This is because the predicted number of antenna elements was always rounded up to some $16L^2$ for an integer value of L where $1 \leq L \leq 8$. This rounding was necessary for each sub-array to fit a square number of MAUs. However, some of the sub-arrays were expanded to fill the remaining empty space in the array. We did not observe any significant adverse effects on detection or tracking when the transmitting sub-arrays were rectangular or L-shaped. A future study could possibly implement a more flexible element allocation algorithm that is based on rectangular sub-arrays rather than squares.

The simulation and algorithms described in this thesis are extremely space and time complex. The simulated radar had a range swathe of approximately 10 kilometers; simulating a wider spread of targets caused the machine running the simulation to run out of memory. All-digital arrays are extremely computationally complex, but they have a lot of potential in target tracking. This thesis has laid the groundwork for more innovation in this new and exciting field.

Bibliography

[1] M. I. Skolnik, "Radar — Encyclopedia Britannica," https://www.britannica.com/technology/radar, November 2020, [Online; accessed 15-June-2021].

[2] C. Fulton, M. Yeary, D. Thompson, J. Lake, and A. Mitchell, "Digital phased arrays: Challenges and opportunities," *Proceedings of the IEEE*, vol. 104, no. 3, pp. 487–503, 2016.

[3] C. A. Recknagel and N. A. Goodman, "Simulation and adaptive sub-array packing for an all-digital phased-array radar," in *2019 IEEE Radar Conference (RadarConf)*, 2019, pp. 1–6.

[4] H. Vann, "Techniques for simultaneous transmit and receive with all-digita arrays," Master's thesis, 2019.

[5] M. A. Richards, *Fundamentals of Radar Signal Processing Second Edition*. McGraw Hill Education.

[6] C. A. Recknagel, "Simulation and adaptive aperture allocation for all-digital phased-array radar," Master's thesis, University of Oklahoma, 2019.

[7] Z. jiankui and Z. junlin, "Study on mimo radar detection performance," in *2009 2nd International Conference on Power Electronics and Intelligent Transportation System (PEITS)*, vol. 2, 2009, pp. 324–326.

[8] J. Li and P. Stoica, "Mimo radar with colocated antennas," *IEEE Signal Processing Magazine*, vol. 24, no. 5, pp. 106–114, 2007.

[9] E. Brookner, "Mimo radar demystified and where it makes sense to use," in *2013 IEEE International Symposium on Phased Array Systems and Technology*, 2013, pp. 399–407.

[10] Z. Jiankui and D. Ziming, "Some mimo radar advantages over phased array radar," in *2010 The 2nd International Conference on Industrial Mechatronics and Automation*, vol. 2, 2010, pp. 211–213.

[11] K. Farnane, K. Minaoui, A. Rouijel, and D. Aboutajdine, "Analysis of the ambiguity function for phase-coded waveforms," in *2015 IEEE/ACS 12th International Conference of Computer Systems and Applications (AICCSA)*, 2015, pp. 1–4.

[12] T. Jeffrey, *Phased-Array Radar Design - Application of Radar Fundamentals*. SciTech Publishing, 2009.

[13] G. V. K. Sharma and K. R. Rajeswari, "Mimo radar ambiguity analysis of phase coded pulse waveforms," in *2012 International Conference on Radar, Communication and Computing (ICRCC)*, 2012, pp. 101–106.

[14] W. L. Stutzman and G. A. Thiele, *Antenna Theory and Design*. John Wiley & Sons, 1981.

[15] S. Z. Gurbuz, H. D. Griffiths, A. Charlish, M. Rangaswamy, M. S. Greco, and K. Bell, "An overview of cognitive radar: Past, present, and future," *IEEE Aerospace and Electronic Systems Magazine*, vol. 34, no. 12, pp. 6–18, 2019.

[16] K. L. Bell, G. E. Smith, A. E. Mitchell, and M. Rangaswamy, "Fully adaptive radar for target classification," in *2019 IEEE Radar Conference (RadarConf)*, 2019, pp. 1–6.

[17] D. Simon, *Optimal State Estimation*, 1st ed. Hoboken (New Jersey): John Wiley & Sons, Inc., 2006.

[18] K. Ramachandra and R. C. Division, "Optimum steady state position, velocity, and acceleration estimation using noisy sampled position data," *IEEE Transactions on Aerospace and Electronic Systems*, vol. AES-23, no. 5, pp. 705–708, 1987.

[19] K. Ramachandra, "Position, velocity and acceleration estimates from the noisy radar measurements," in *IEE Proceedings*, vol. 101, no. 2, 1984, pp. 167–168.

[20] A. Macaveiu and A. Câmpeanu, "Automotive radar target tracking by kalman filtering," in *2013 11th International Conference on Telecommunications in Modern Satellite, Cable and Broadcasting Services (TELSIKS)*, vol. 02, 2013, pp. 553–556.

[21] D. F. Crouse, "A crash course in basic single-scan target tracking," 2017, slideshow presented to Radar Division and approved for public release.

[22] V. T. Dang, "An adaptive kalman filter for radar tracking application," in *2008 Microwaves, Radar and Remote Sensing Symposium*, 2008, pp. 261–264.

[23] S. Martello and P. Toth, *Knapsack Problems: Algorithms and Computer Implementations*. John Wiley & Sons, Ltd, 1990.

[24] L. Epstein, "Two-dimensional packing with conflicts," *Acta informatica*, vol. 45, no. 3, pp. 155–175, 2008.

[25] D. Pisinger, "Algorithms for knapsack problems," 1995.

[26] G. W. Stimson, *Introduction to Airborne Radar*, 2nd ed. SciTech Publishing, 1998.